DESIGN OF A LOAD CELL FOR TRIAXIAL FORCE MEASUREMENT IN WALKING

by

Robert Gregory Clarke

SUBMITTED TO THE DEPARTMENT
OF MECHANICAL ENGINEERING
IN PARTIAL FULFILLMENT OF THE
REQUIREMENTS FOR THE
DEGREE OF

BACHELOR OF SCIENCE

at the
MASSACHUSETTS INSTITUTE OF TECHNOLOGY
June 1981

Signature of Author .....

Department of Mechanical Engineering
May 20, 1981

Certified by .....

Woodie Flowers
Thesis Supervisor

Accepted by .....
Thesis Review Committee

DESIGN OF A LOAD CELL FOR TRIAXIAL FORCE MEASUREMENT IN WALKING

by
ROBERT GREGORY CLARKE

Submitted to the Department of Mechanical Engineering on May 20, 1981, in partial fulfillment of the requirements for the Degree of Bachelor of Science.

ABSTRACT

In response to the need to measure foot-floor reaction forces in gait analysis, a system was designed using load cells mounted on the bottom of the shoe.

A review of current foot-floor force measuring systems and of the requirements for an ideal system led to the development of a concept using shoe-borne instrumentation.

The system consists of five load cells placed on the bottom of each foot, wired to a backpack which contains all the required system instrumentation. The load cell is machined from a single block of aluminum one inch square and .40 inches thick. Twelve strain gages are placed on four load bearing columns to yield triaxial force information.

A load cell was constructed and calibrated. The calibration showed good sensitivity for a wide range of axial and shear loads. The load cell also showed reasonable linearity. The resolution of the system tested was not very high but could be improved by greater amplification.

Recommendations are made for further testing and revisions in the design.

Thesis Supervisor: W.C. Flowers

ACKNOWLEDGEMENTS

I wish to thank the supervisor of this thesis, Professor Woodie Flowers, for his assistance and unending patience throughout the project. I would also like to thank Elizabeth McInerney for typing the document, and perhaps more importantly, for her constant moral support.

TABLE OF CONTENTS

LIST OF FIGURES

LIST OF TABLES

CHAPTER 1: INTRODUCTION

1.1 Brief Overview of the Project

An individual's ability to function effectively in his environment depends largely upon gait. The study of gait mechanics requires knowledge of the foot-floor reaction forces. A history of the many methods used to try to determine these forces is given by Estey (8). Although a force plate is normally used, it is advantageous to use shoe-borne instrumentation. This thesis is a report of the design of a new dynamic force-measuring system for gait analysis. A possible use of the system is in a clinical setting for gait analysis of amputees with above-knee prostheses. The work was done as part of the M.I.T. Knee Project in the Mechanical Engineering Department under the supervision of Professor Woodie Flowers.

Current foot-floor reaction forces are usually determined by using a force plate. The force plate is limited in that it can obtain data for only one or two steps in a restricted area. This may inhibit a subject's gait. In addition, force plates are generally quite expensive.

The force measuring system proposed in this thesis consists of five small load cells on each foot. The load cells are mounted on the bottom of the shoe beneath

anatomical landmarks on the foot. The load cells would determine dynamic triaxial force information at five different points on the foot. All other necessary instrumentation would be carried by the subject in a backpack.

Strain gages were chosen as the force transducer after consideration of several alternatives. A strain-gaged load cell was designed, constructed, and tested.

CHAPTER 2: DESIGN CONCEPT

2.1 Concept and Requirements for Design

Many different force measuring systems have been designed and built by researchers and physicians. Estey (8) describes many of these methods and mentions many of the difficulties experienced. This chapter describes the general approach taken by the author to solve this problem as a participant in the M.I.T Knee Project. The M.I.T. Knee is a microprocessor-controlled above-knee prosthesis for amputees. This project would benefit from a new force measuring system for gait analysis of amputees using the prosthesis.

From the outset, an attempt was made to design instrumentation which would be shoe-borne rather than contained in a force plate. A force plate, while not having stringent size and weight constraints, has several inherent disadvantages. A force measuring system should allow for free movement of the subject. A force plate requires the intersection of the subjects's path with the plate, inhibiting free movement and possibly invalidating the data. In addition, the force plates are not easily moved about. Properly designed foot-borne instrumentation could obtain data for different activities in settings outside of the

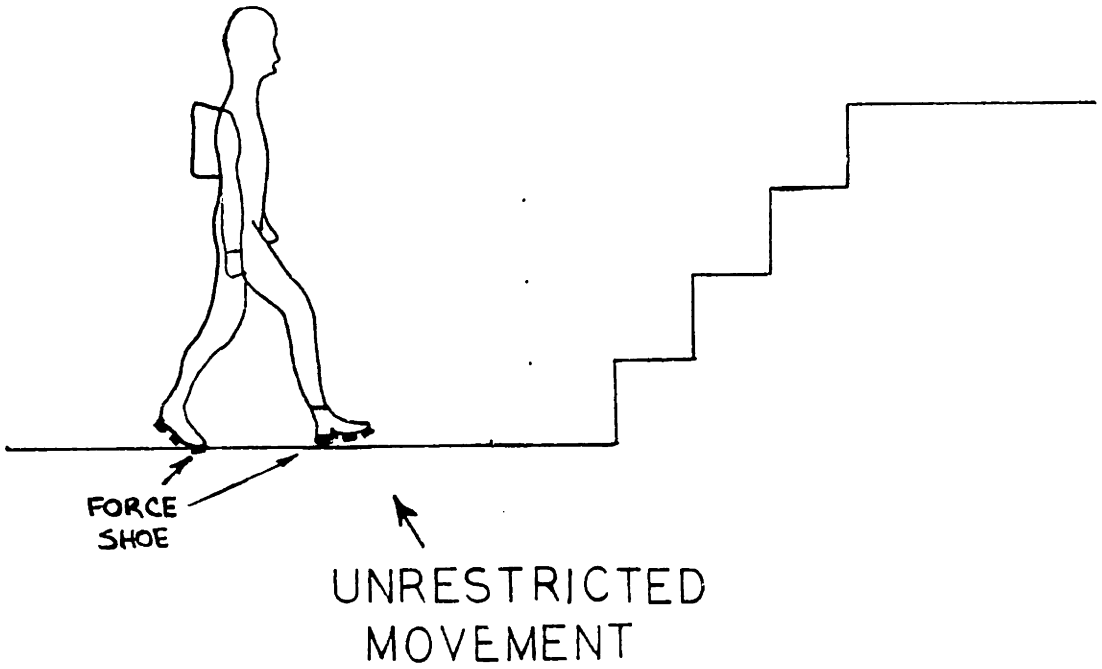

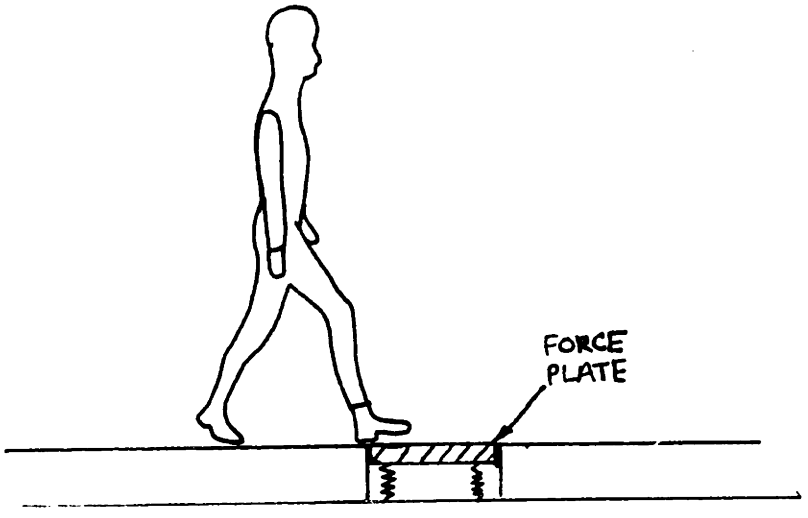

Figure 2.1

Force Plate Versus Force Shoe

laboratory. Figure 2.1 illustrates the value of shoe-borne load cells.

A good beginning for understanding the requirements of a force-sensing shoe is to look at the characteristics of an ideal system. The ultimate shoe would not, in any way, alter the gait of the individual and could be used anywhere at anytime. It would be easily applied and removed and have zero volume and weight. It would transduce the force in three directions at every point on the shoe and telemeter the data to a computer. It would be linear and have infinite frequency response. Of course, it would be free.

The practical force-shoe will be a compromised version of the ideal shoe. The ability to obtain triaxial force information was considered a necessity for the device. Amputees often drag their prothesis, especially when first adapting to it, so shear force data is valuable in assessing this aspect of amputee gait.

There is a trade-off between the number of points of force information and the corresponding value. One hundred transducers would produce useful information, but also requires 100 sets of wires. In addition, this wealth of data is not easily expressed in a form simple enough to be of use. Since feet vary so greatly in size, it would be difficult to design a system to take a large number of data points which is adaptable to all shoes.

The system should take force data beneath anatomical

landmarks to allow correlation of data for different subjects. This also permits relatively accurate placement on the same subject's foot on different occasions. The placement of the load cells would be under bony weight-bearing protuberances, making their presence almost undetectable. The load cells should be under the bones that bear the most normal load, to provide for sufficient support and balance. Although this will provide only pointwise information, the points give a good approximation of the actual physical support method. According to the work of Dhanendram (6), support while walking is provided by the big toe, the third and the fifth metatarsals, and the heel. Therefore, five load cells will be placed on the bottom of the shoe: one each under the big toe and the third and the fifth metatarsals, and two under the heel.

The desired size of the load cells can be estimated. Contini (3) gives the average size of human feet in Table 2.1.

TABLE 2.1

Foot Dimensions for Normal Humans

MEN:	Foot Width	= .055 x Height
	Foot Length	= .152 x Height
WOMEN:	Foot Width	= .057 x Height
	Foot Length	= .151 x Height

It is advantageous to have subjects as small as four feet

tall, with a foot width of about 2.7 inches. A survey of five hard-soled shoes showed that the width of the heel of the shoe is about three-quarters of the foot width and the length of the heel about one-third of the foot length. The heel for a four foot person would be about 2 by 2 1/4 inches. A load cell with larger than a one-inch diameter would overhang the shoe and not be fastened as securely.

The thickness of the load cells should be as small as possible. Under one-half inch thick would be acceptable. The author walked on one inch diameter by half inch thick blocks and found them satisfactorily comfortable.

The load cells must endure maximum loads of 500 pounds in the vertical direction, 140 pounds in the fore-aft direction, and 25 pounds in the lateral direction. These figures are roughly twice those expected from the normal gait of a 225 pound man (8) and allows for the possible case of different activities. At the same time, the load cells should have a resolution of one pound. According to Holden and Muncey (11), the highest frequency of these forces during walking is 500 hz. The system must have a natural frequency greater than this.

The load cells should be mounted on the shoes in a rigid fashion to allow accurate transmittal of forces. Other important considerations include durability, weight, and manufacturability. Aluminum was chosen as the load cell material since it is lighter and easier to machine than

steel.

The signals from the load cell will be wired to a backpack containing the necessary electronics to condition the signals, convert them to digital, and store them for input to a computer.

2.2 Strain Gage as Transducer

Numerous transducers were studied for possible use in the load cell. These included variable resistance strain gages, piezoelectric crystals, variable capacitance devices, linear variable displacement transformers (LVDT), optical detection devices, and electrically conductive elastomers. The desire to obtain triaxial force output, combined with their relative simplicity, small size, and proven reliability, made strain gages the logical choice for this application.

Strain gages operate on the principle that the resistance of a wire changes when its length and cross-sectional area change. The initial resistance of the wire is:

$$R = \frac{\rho L}{A}$$

where:

ρ = resistivity of material
L = length of wire
A = cross-sectional area of wire

Under tension or compression the wire changes resistance:

$$\Delta R = \frac{\rho \Delta L \ (1 + 2\nu)}{A} + \frac{L \Delta \rho}{A}$$

where:

ν = Poisson's ratio for material

The gage factor GF is defined as the fractional change in resistance divided by the fractional change in length:

$$GF = \frac{\Delta R/R}{\Delta L/L} = (1 + 2\nu) + \frac{\Delta \rho / \rho}{\Delta L/L}$$

The first quantity represents the effect of dimensional change. Since Poisson's ratio is about .3 for most metals, the gage factor would only be about 1.6 if this were the only factor. Since most gage factors are around 2.0, the second term, known as the piezoresistive effect, has cosiderable impact on this value.

The semiconductor gage was developed in the 1950's. It has extremely high gage factors in the range of 110-150, due mainly to the piezoresistive effect. Unfortunately, semiconductor gages are highly temperature dependent and non-linear.

The two main types of gages are resistance wire and metal foil. Resistance wire gages are typically .001 inches in diameter and cemented to a paper backing. Foil gages have ribbons as small as 4×10^{-4} inches in diameter and are mounted on a thin epoxy ethylene backing. Foil gages have generally superior characterisics, such as better bonding, greater heat dissipation, higher current carrying capacity,

and greater stability.

The gage is cemented to the material in which it measures the strain along the axis of the wires. Small lengths of the conductor where the wire turns imparts some transverse sensitivity, which is usually neglected. This is about 2% in wire gages and .2% in foil gages.

The gages must be used in Wheatstone Bridge circuits for small changes in resistance. Either A.C. or D.C. current can be supplied. Chapter 3 contains more details on bridge circuits.

With quality electronics, strains as low as 10^{-7} in/in can be readily detected. This lower limit is due to thermal noise, a white noise generated by electron motion in the gage.

Thermal efects are proportional to the cube of the gage current. The effect where the circuit balance is altered by differential heating of the bridge arms is called D.C. drift. While gages are made which are self temperatyre compensated for a certain range, gages normally have a temperature coefficient of resistance of $10\text{-}15 \times 10^{-6}/^{o}C$. This is extremely important in static testing, while having little effect in dynamic applications.

CHAPTER 3: DESIGN OF LOAD CELL

3.1 Geometry of Load Cell

Several possible geometries for the load cell were considered which could yield triaxial force information in this application. The basic configurations are a single column, a single thin-walled cylinder, and multiple columns or cylinders.

A solid column would have to be relatively thin as in Figure 3.1 to strain a measurable amount under our loads. There are problems with this configuration due to end effects. Consider an axial force applied at the edge of the unrestrained plate. It is obvious that there will be considerable bending of the column. The strain gages would not be able to differentiate between this strain and a strain due to shear force which also bends the column.

A single thin walled cylinder with an outer radius of one-half inch and a thickness of .33 inches is acceptable as far as response requirements and load limits.

A multiple column or thin-walled cylinder arrangement is also acceptable for response and load limits. A four column arrangement is ideal since it allows the column to be placed along the shear axes. Shear forces can be read directly. The symmetry involved is also helpful for cancelling out undesired strains, as seen later.

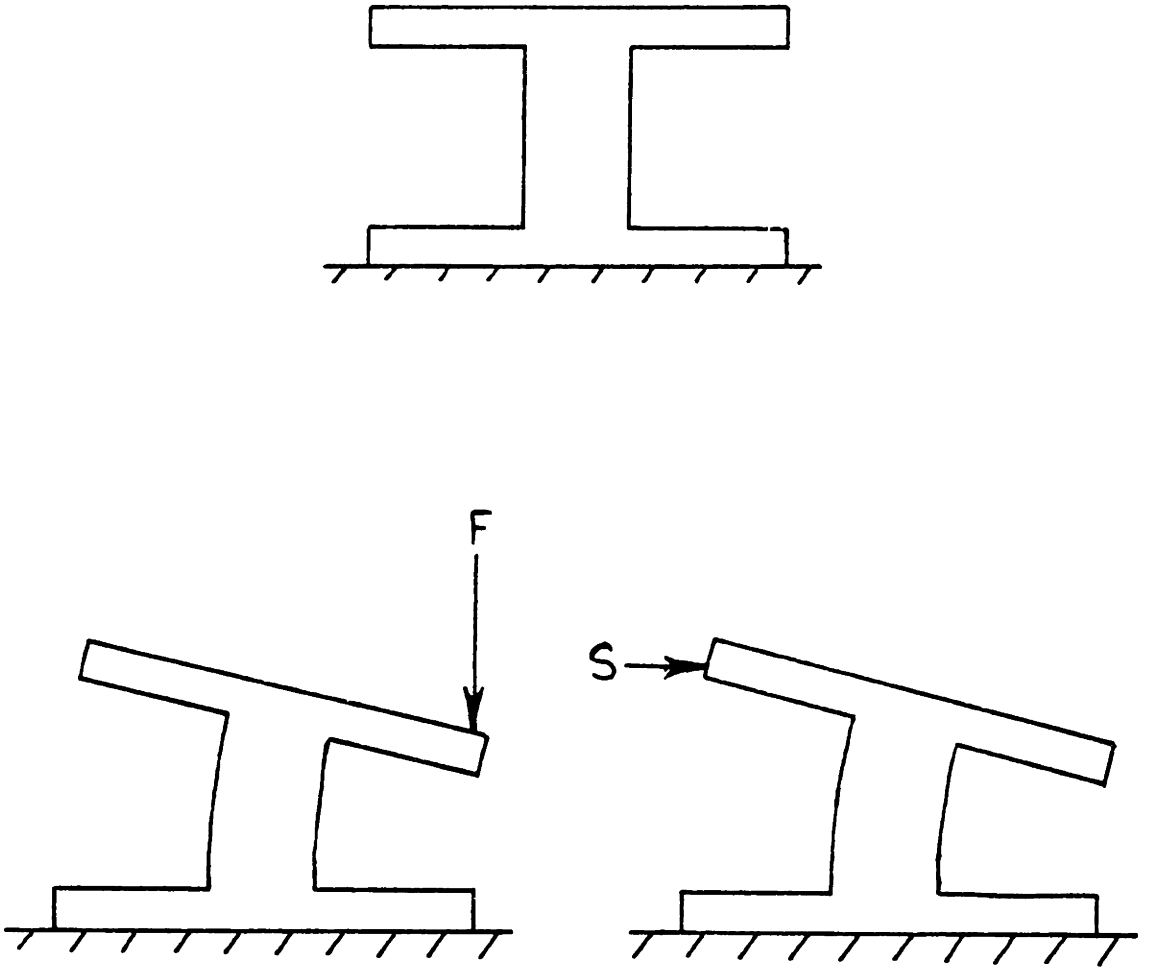

Figure 3.1

Loading of a Single Column Lead Cell

A most important factor is the ease of manufacturing. The load cell can be machined as a single piece, or as several parts and fastened together. Brazing is a possible fastening method, but it is very difficult to do with any accuracy and creates a joint of questionable strength. Screws create stress concentrations and add to the thickness of the load cell with the head. A single piece load cell avoids these problems. The four column load cell is the most practical geometry for single block construction.

Possible geometries for four load bearing columns are shown in Figures 3.2 to 3.4. An analysis of bridge circuit configurations indicates that twelve gages should be placed on the load cell on three sides of every column. Three sides of every column in Figure 3.4 are accesible for placement of gages. Eight of the gages are on the interior for protection of the gages. In addition, the machining is straightforward enough to merit the choice of this geometry for the load cell.

3.2 Load Cell Details

The dimensions of the load cell can now be determined. Consider the triaxially loaded column of Figure 3.5. The force F is resolved into a longitudinal component T and transverse components N and M. It is assumed that the column is relatively stiff, so that its bending deflection

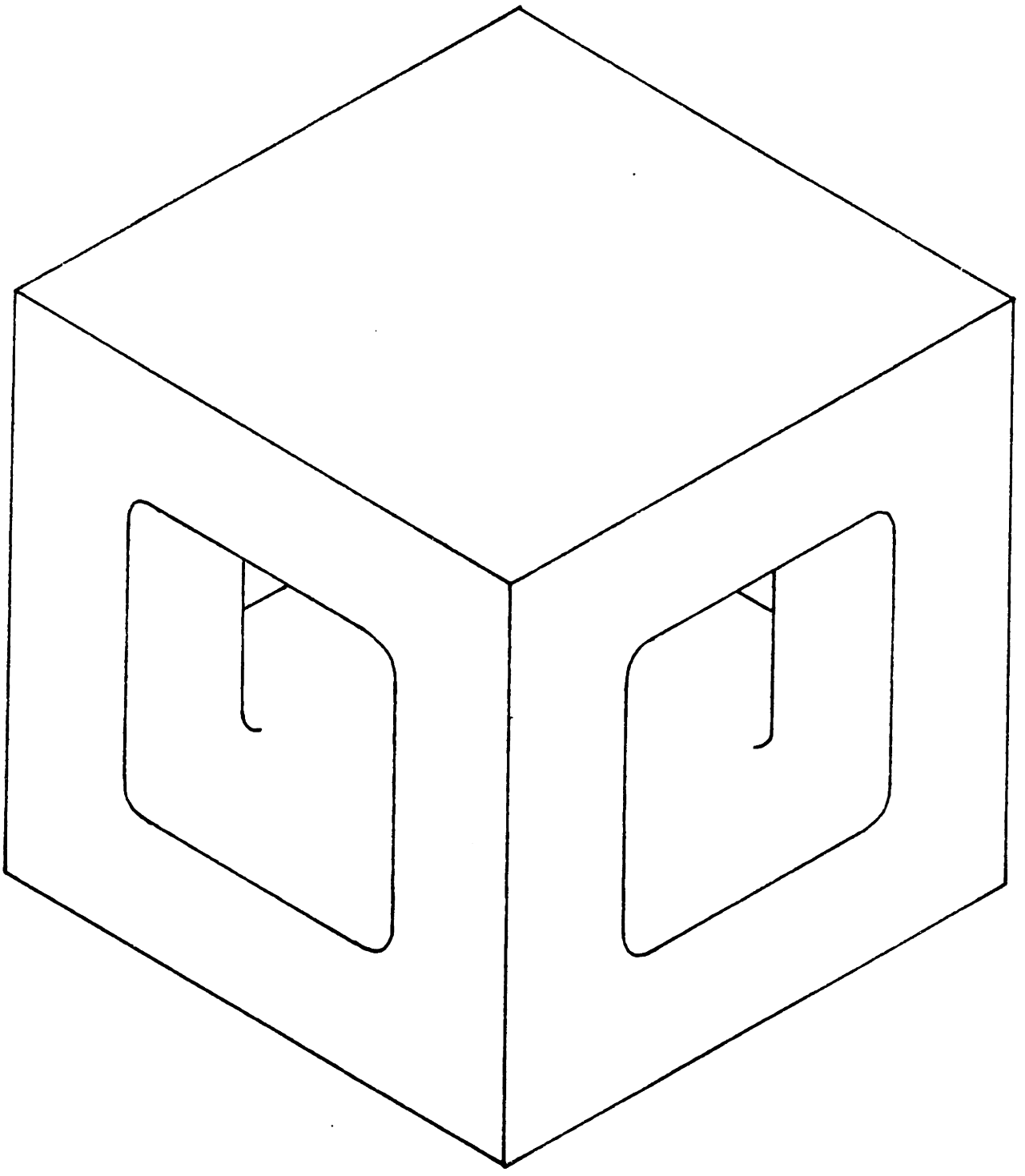

Figure 3.2

Alternative Load Cell Geometry

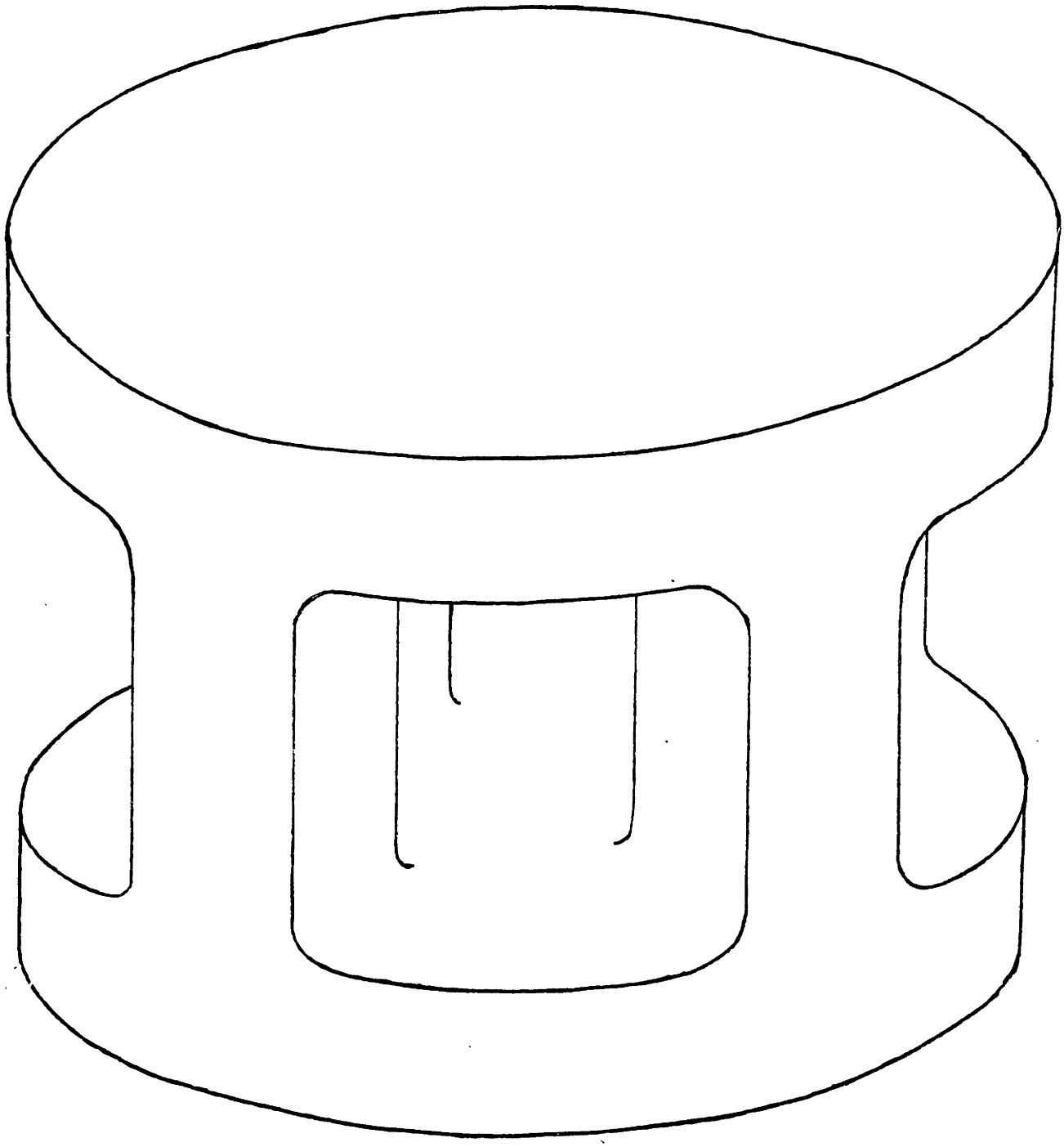

Figure 3.3

Alternative Load Cell Geometry

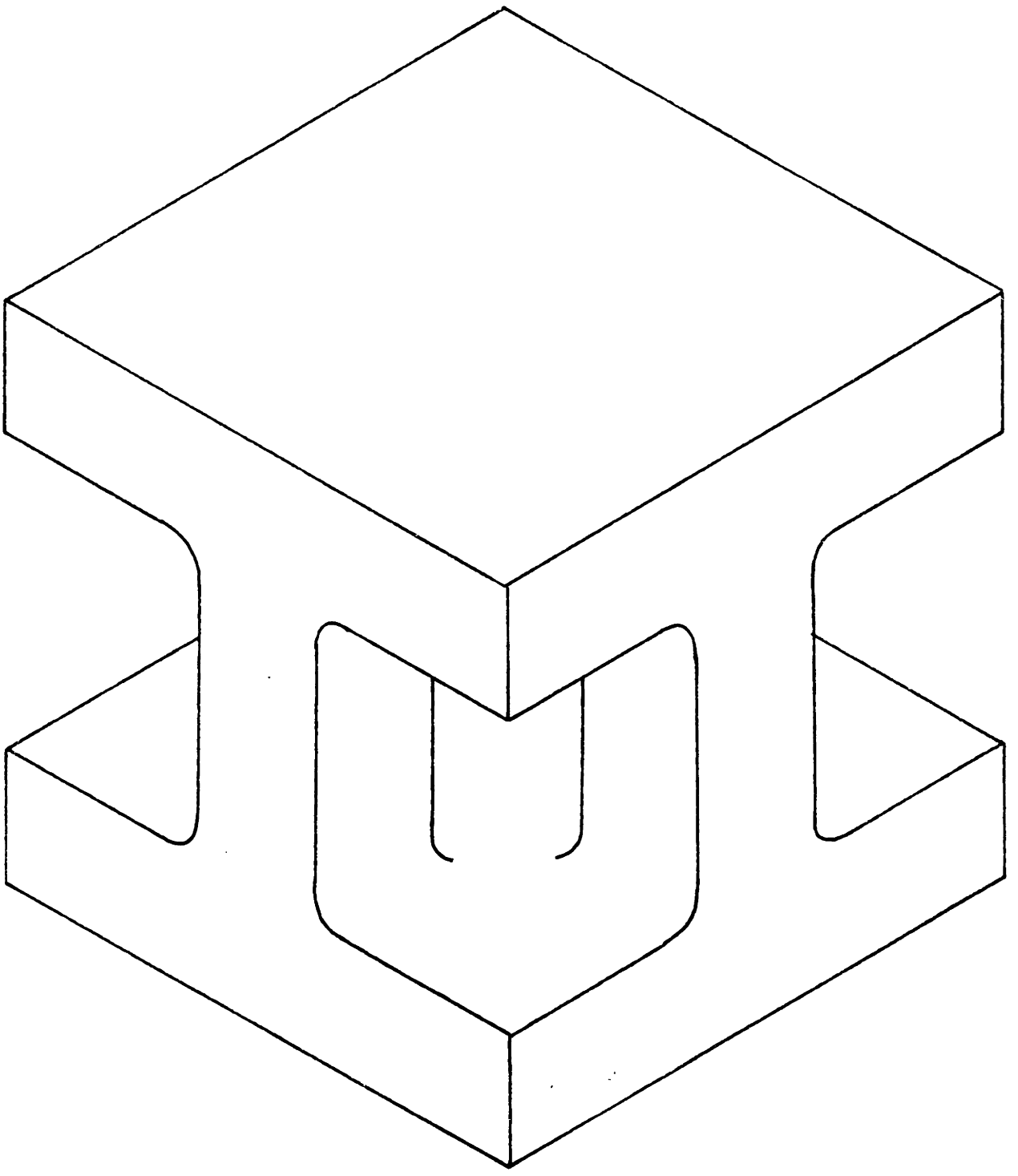

Figure 3.4

Chosen Load Cell Geometry

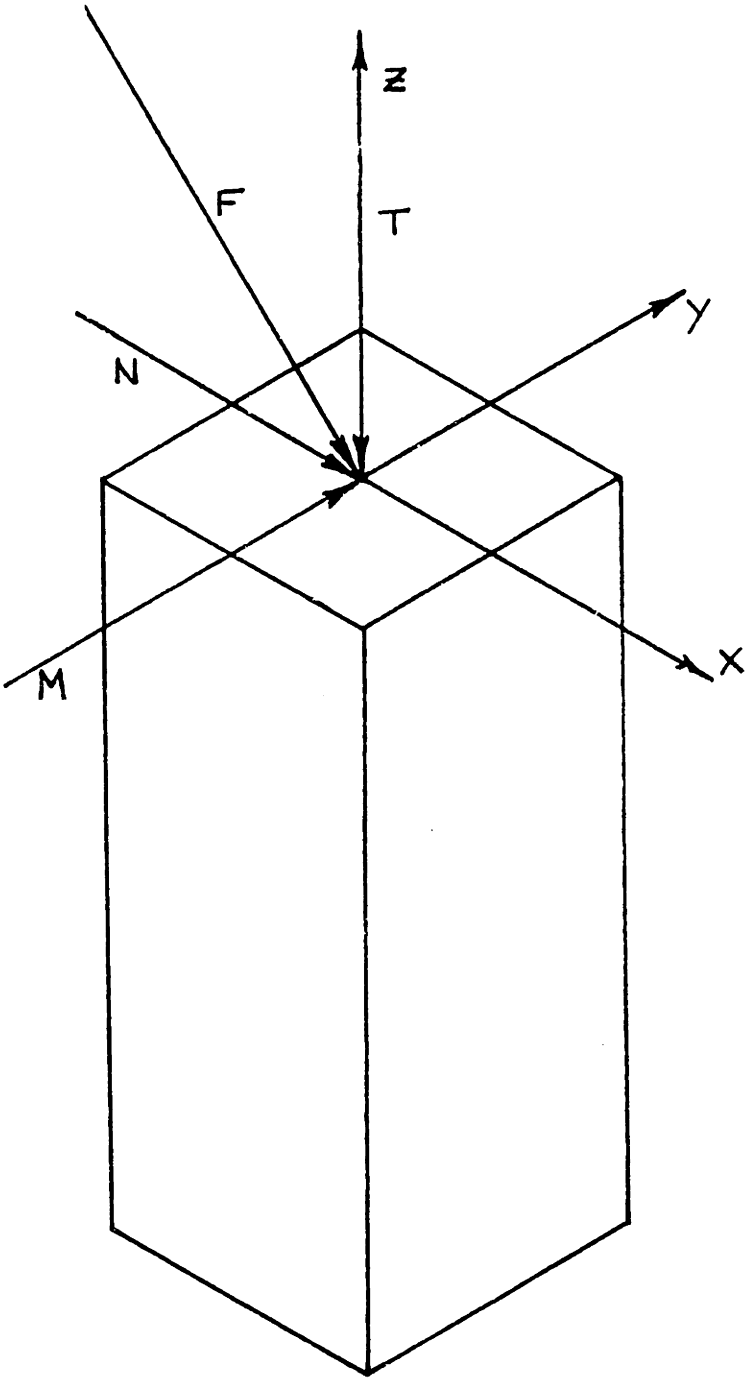

Figure 3.5

Triaxially Loaded Column - Restrained at One End

is so small as to be negligible. The stress at any point is obtained by superimposing the compressive stress on the bending stresses from the shear loads. Timoshenko (19) gives the resultant stress along the z-axis:

$$\sigma = -\frac{Mly}{I_x} - \frac{Nlx}{I_y} - \frac{T}{A}$$

where:

M = shear force in y-direction
N = shear force in x-direction
l = distance from top of column
x,y = distance from column center
I_x, I_y = moment of inertia
T = thrust force in z-direction
A = cross-sectional area of column

The maximum stress, σ max, occurs at the bottom of a beam on its outer surface. For four square columns with sides of length b:

$$\sigma \text{ max} = \frac{-N\ L\ (b/2)}{4\ (b^4/12)} - \frac{M\ L\ (b/2)}{4\ (b^4/12)} - \frac{T}{4\ b^2}$$

where L = length of column

The length of the column was set at .285 inches to allow room for the gages and the lead wires. For 2024 aluminum, the maximum stress recommended by (5) for transducer operation is 10,000 psi. A load cell with columns .18 inches square will develop a maximum stress of 9300 psi.

The desired resolution of the load cell is one pound. Cook gives the limit of strain resolution as 10^{-7} in/in while 10^{-6} in/in is probably more typical of what can be expected.

For an axial force of one pound, the strains developed in the gages are:

(3A)
$$\epsilon\,(\text{axial}) = \frac{\sigma\,(\text{axial})}{E} = -\frac{1}{4\,b^2} \cdot \frac{1}{E} = 7.7 \times 10^{-7} \text{ in/in}$$

where:
E = modulus of elasticity for aluminum = 10×10^6 psi

This approaches the practical limits of strain resolution. For a shear force of one pound, the gages are subjected to a strain:

(3B)
$$\epsilon\,(\text{shear}) = \frac{\sigma\,(\text{shear})}{E} = \frac{1}{4}\,\frac{1(b/2)}{(b^4/12)} \cdot \frac{1}{E} = 2.1 \times 10^{-6} \text{ in/in}$$

where:
l = distance from top of column to center of strain gage grid = .18 inches

This resolution is within the achievable limits.

To prevent edge effects and minimize bending of the floor contact plate, much of the unsupported plate should be removed. Material should be removed from the corners in the shape of isosceles triangles with sides of about .25 inches. In addition, a hole about .3 inches in diameter should be drilled through the plate to reduce the unsupported

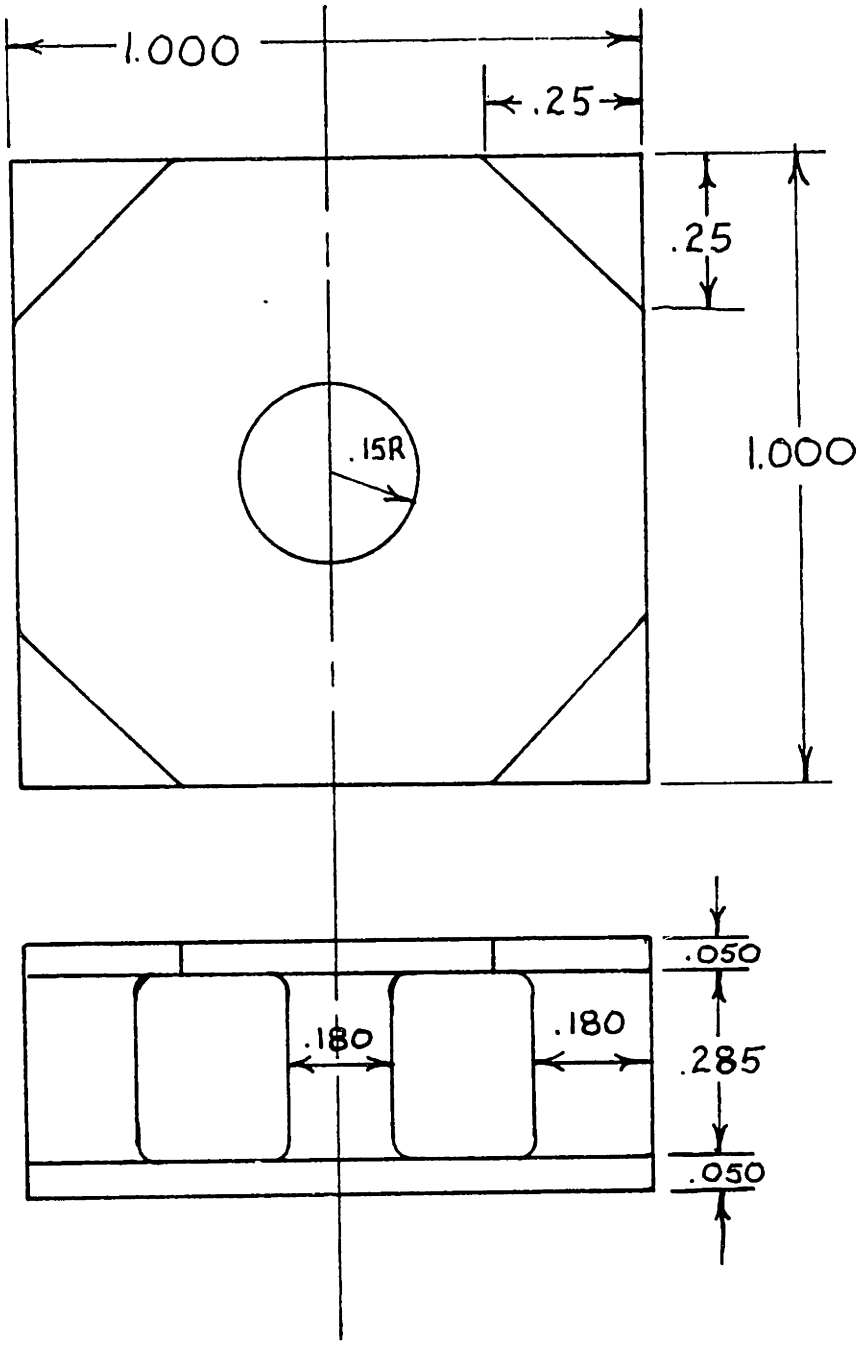

Figure 3.6

Dimensioned Load Cell

overhang in the center. The endplates should have a thickness of about .050 inches. The dimensioned load cell is shown in Figure 3.6.

An important aspect of the design is the mounting of the load cell on the shoe. The rigidity of the mounting will have an effect on the accuracy of the force transmitted to the shoe and also on the natural frequency of the system. The simplest method is to use epoxy to attach the load cell to the shoe. A subject would first walk with the load cells adhered to the shoe by putty. The load cells are moved around until the subject is comfortable and then their position is marked. The surfaces are cleaned and the load cells epoxied to the shoe in that position. This method is easy and quick. Alternative methods are possible using fasteners such as screws, but these require that the shoe be altered in a permanent manner. This would prevent the subject from walking in the shoes that he normally uses and may change the subject's gait.

The strain gages and wire leads must be protected from the environment. Figure 3.7 shows the proposed terminal loops. This is similiar to a product of BLH Electronics but is shorter. The strip is cemented to the load cell. The gage leads are soldered on one end and the lead wires are mechanically fastened and soldered. Short lengths (1 - 2 inches) of 27 AWG stranded copper wire leave the load cell and are spliced into 22 AWG stranded copper wire. This wire

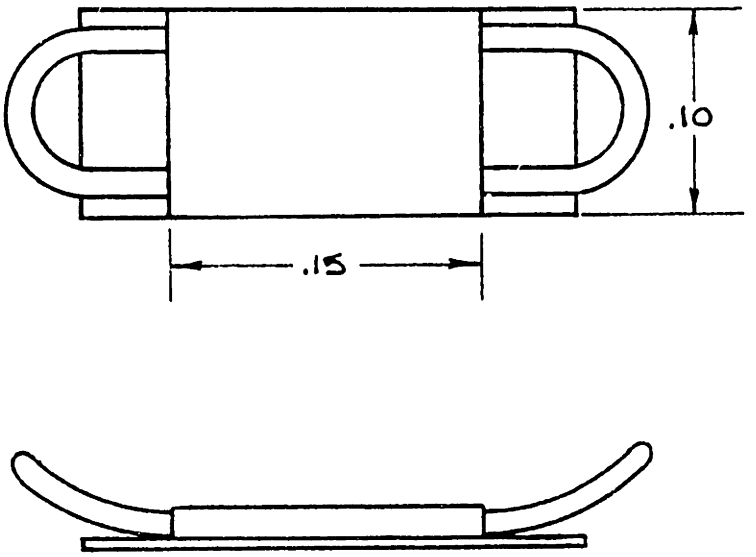

Figure 3.7 Proposed Terminal Loops

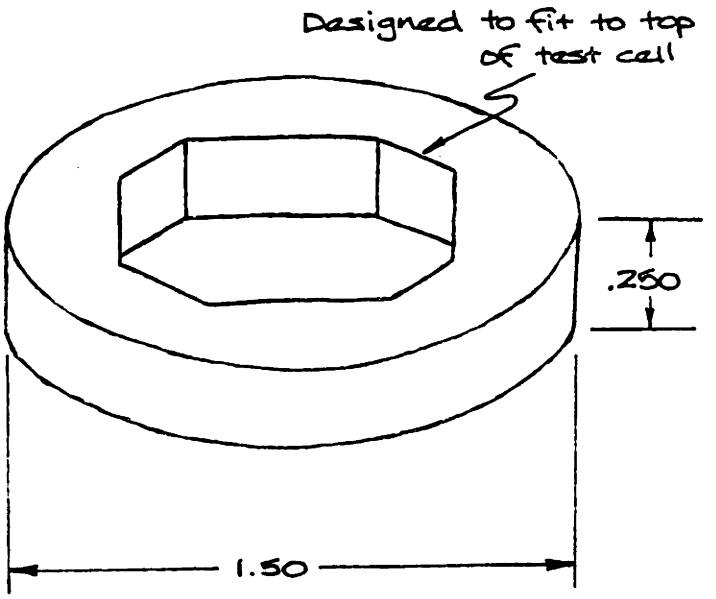

Figure 3.8 Plastic Cover for Load Cell Protection

is polypropylene insulated with a vinyl jacket to prevent excess noise pickup. The 27 AWG wire protects the strain gage leads. If the outer wires are pulled, the 27 AWG wire will snap before the terminal breaks off, preventing the gage leads from being pulled off.

The plastic cover of Figure 3.8 should be placed around the outside of the load cell for protection of the gages and leads. The cover is epoxied on to the load cell and has holes for outside wire leads.

The proper strain gage is a FAE-06S-12S13-EL from BLH Electronics, shown in Figure 3.9. This is a 120 ohm, 2.03 gage factor, constantan foil gage on a polymide backing. The gage is encapsulated for protection and stability and the leads are already soldered on. The gage is temperature compensated for aluminum. A plot of temperature induced error versus temperature is shown in Figure 3.10.

3.3 Bridge Circuit Theory and Application

Strain gages are typically arranged in Wheatstone bridge circuits as in Figure 3.11. The resistances are provided by active strain gages, "dummy" or temperature compensation gages, or standard resistors. The choice of the gage arrangement varies for each application.

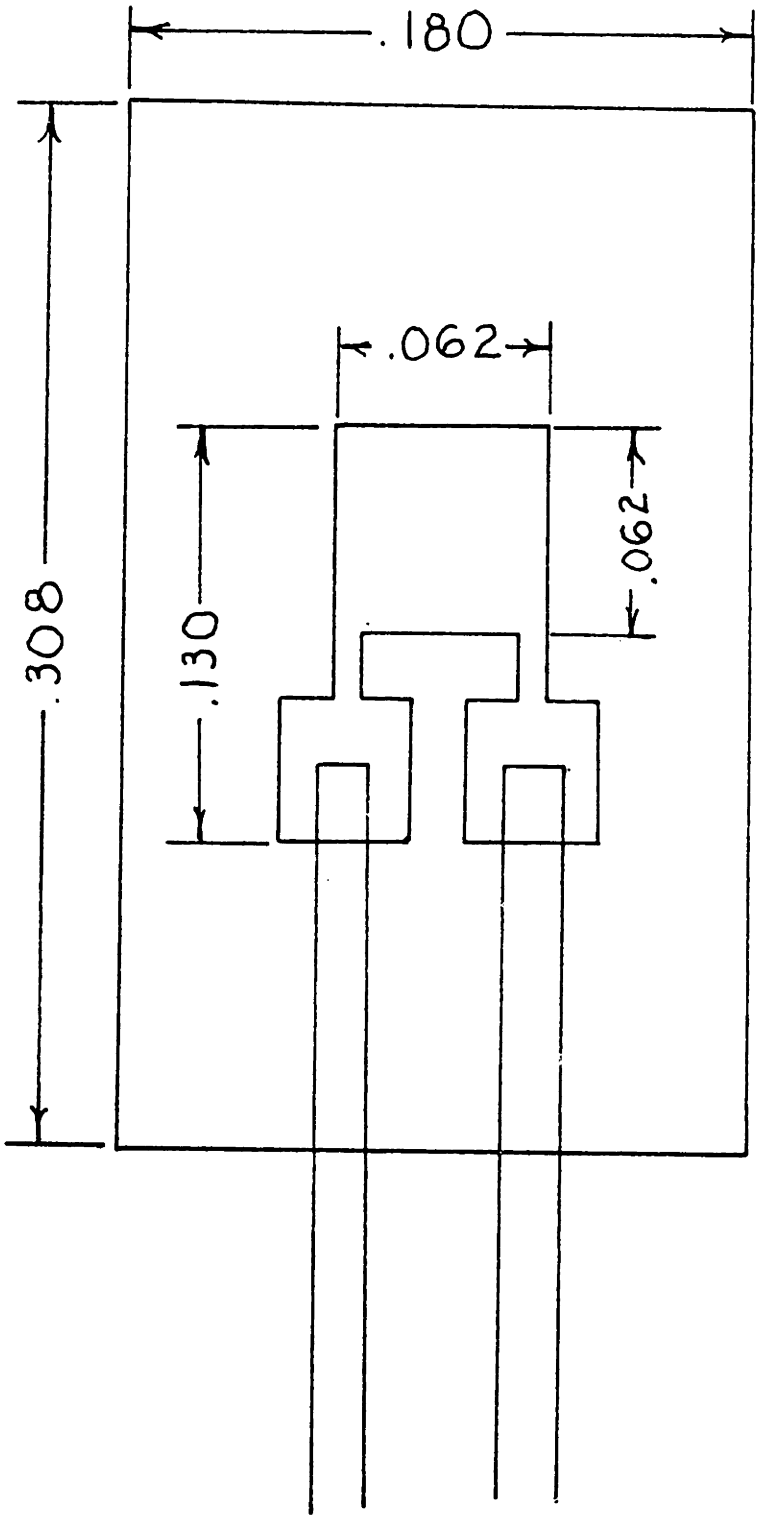

Figure 3.9

FAE-06S-12513-EL Strain Gage

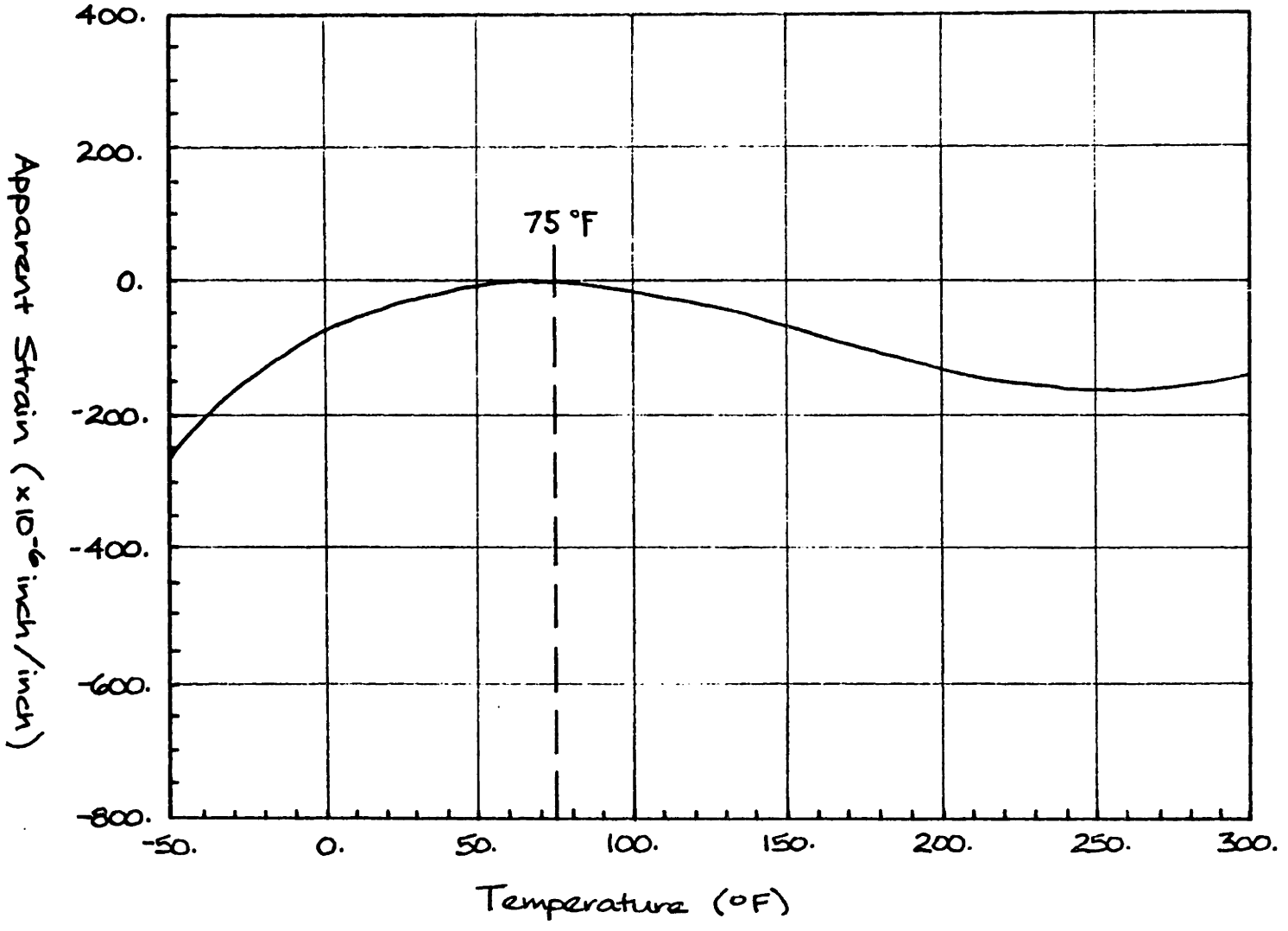

Figure 3.10

Temperature Compensation for FAE Gages on 2024 Aluminum

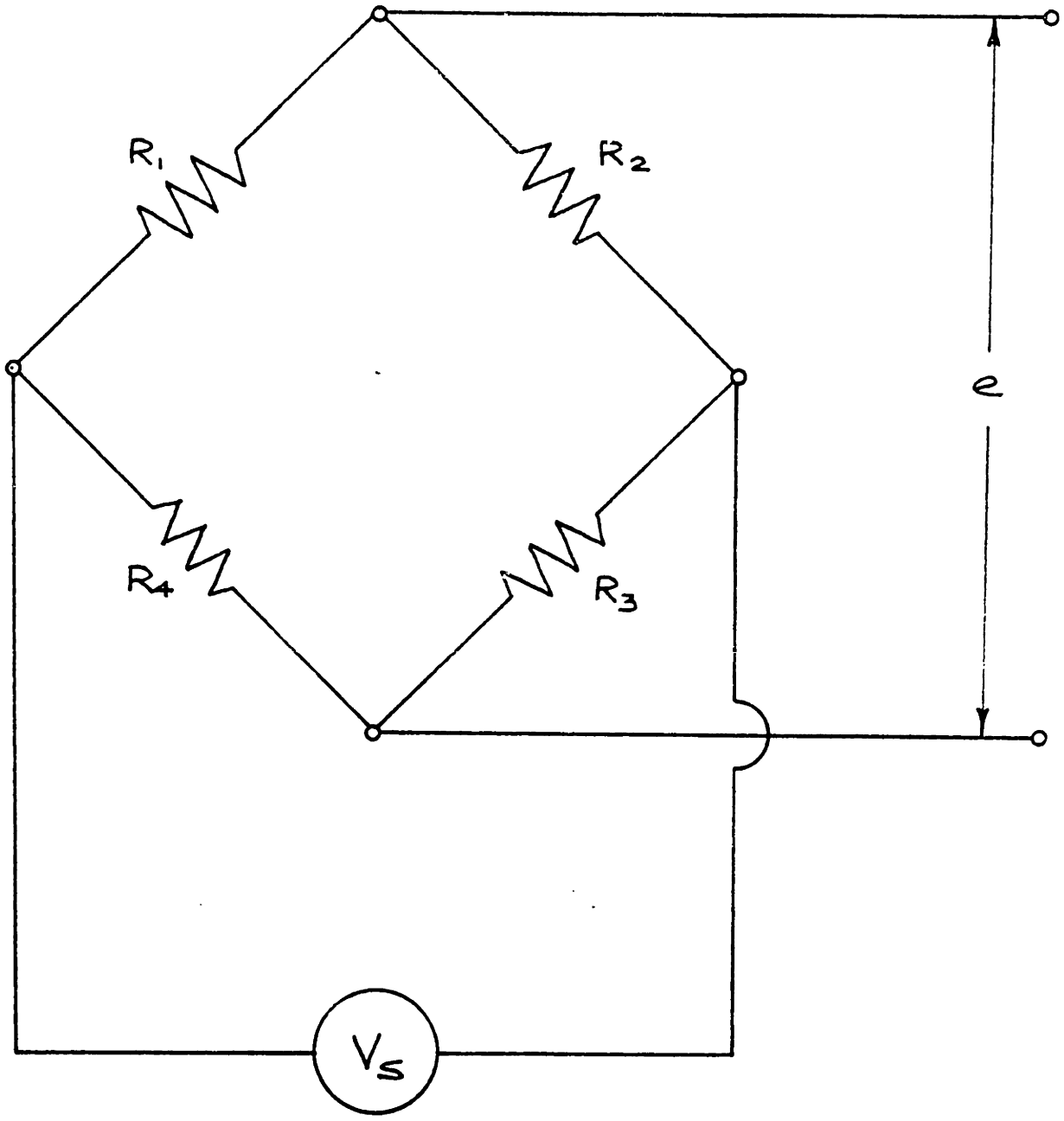

Figure 3.11

Wheatstone Bridge

Application of Kirchoff's Law gives the output equation for the bridge. Assuming that the oscilloscope draws no current (infinite impedance):

$$e = V_S \frac{R_1 R_3 - R_2 R_4}{(R_1+R_2)(R_3+R_4)}$$

where:

e = output voltage of bridge
V_S = voltage source
R_N = resistance in Nth arm of bridge

When the circuit is balanced, $R_1 R_3 = R_2 R_4$ and the bridge output is zero. For changes in the resistance of each gage:

$$\Delta e = V_S \frac{(R_1+\Delta R_1)(R_2+\Delta R_2) - (R_3+\Delta R_3)(R_4+\Delta R_4)}{(R_1+\Delta R_1+R_2+\Delta R_2)(R_3+\Delta R_3+R_4+\Delta R_4)}$$

where:

ΔR_N = resistance change in Nth arm of bridge
Δe = change in output voltage

This can be simplified for ΔR much smaller than R.

$$(3C) \quad \Delta e = V_S \frac{R_1 R_3}{(R_1+R_2)(R_3+R_4)} \left(\frac{\Delta R_1}{R_1} - \frac{\Delta R_2}{R_2} + \frac{\Delta R_3}{R_3} - \frac{\Delta R_4}{R_4} \right)$$

For a given circuit, this can be rewritten as:

$$(3D) \quad \Delta e = C\left(\epsilon_1 - \epsilon_2 + \epsilon_3 - \epsilon_4 \right)$$

where:

C = constant $= V_S \frac{R_1 R_3}{(R_1+R_2)(R_3+R_4)} \cdot GF$

ϵ_N = strain in Nth arm of bridge $= \frac{\Delta R_N}{R_N} \cdot \frac{1}{GF}$

The present application requires triaxial force output for a symmetrical four column arrangement. Space constraints give a practical limit of one gage per column. Twelve 120 ohm active gages are used, placed on the columns as in Figure 3.12. The gages must be accurately placed axially at the center of the columns on the same horizontal level.

Gages 3,6,9, and 12 are arranged in a bridge circuit as in Figure 3.13. If the center of the load cell is subjected to an axial thrust load P, each gage is deformed by an equal amount:

$$\epsilon_a = \frac{P}{E}$$

where: ϵ_a = axial strain
E = modulus of elasticity

Using equation (3D), the output of the bridge becomes:

$$\Delta e = C(\epsilon_1+\epsilon_3) = C\left[(\epsilon_a+\epsilon_a) + (\epsilon_a+\epsilon_a)\right] = 4C\epsilon_a$$

The output of the bridge is four times that of a single 120 ohm gage and is proportional to the applied load for a constant modulus of elasticity. If the load is applied off center, the circuit effectively averages the strain in all four gages to produce the same output.

The axial force output is independent of shear forces applied to the load cell as in Figure 3.14. If the top plate is rigid, two

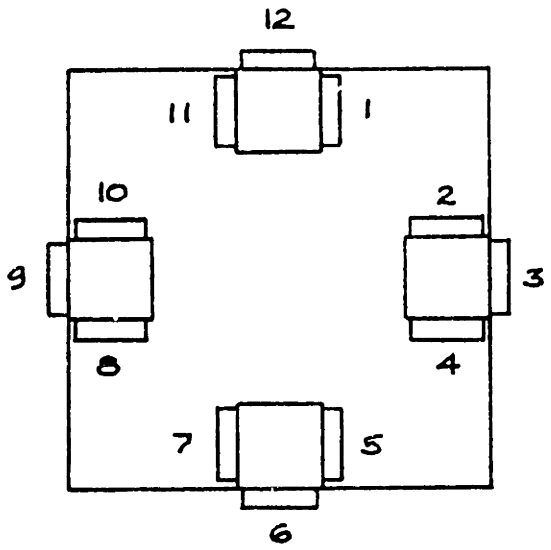

Figure 3.12 Placement of Strain Gages on Load Cell

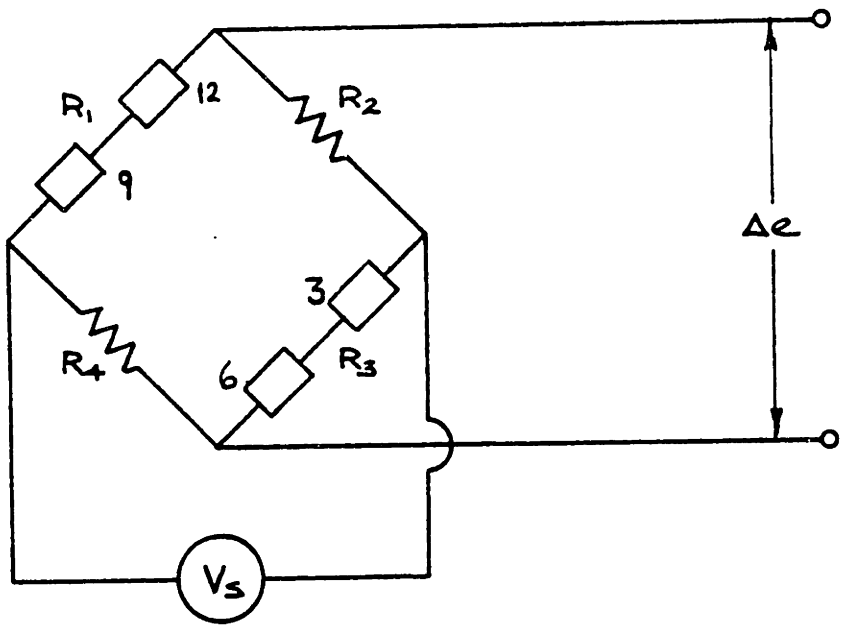

Figure 3.13 Bridge Configuration for Axial Force Measurement

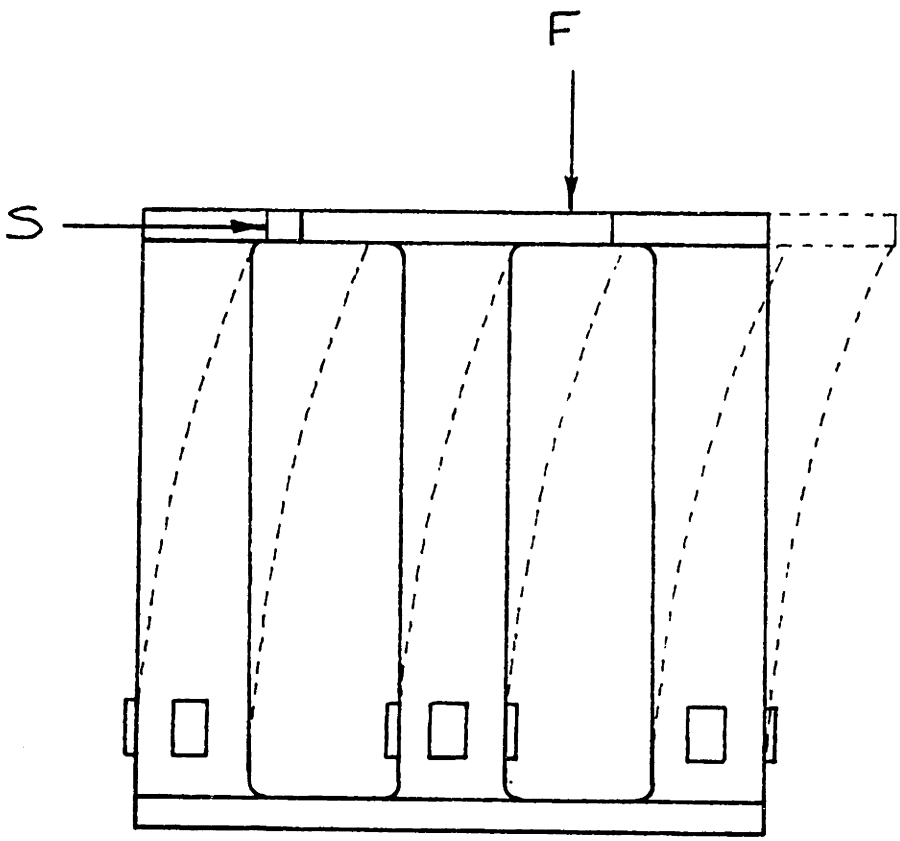

Figure 3.14

Load Cell in Combined Loading

identical columns on opposite sides of the load cell will bend an equal amount when the shear force S is applied. Gages on opposite sides of the load cell will be subjected to strains of equal magnitude but opposite sign such that:

$$\epsilon_{g3} = -\epsilon_{g9} \text{ and } \epsilon_{g6} = -\epsilon_{g12}$$

where ϵ_{gi} = strain in ith gage as numbered in Figure 3.12.

Substitution of these values into equation (3D) shows that the response to shear force is zero.

$$\Delta e = c\left[(\epsilon_{g3} + \epsilon_{g6}) + (-\epsilon_{g3} - \epsilon_{g6})\right] = 0$$

The output is also independent of torsion, as illustrated in Figure 3.15. In this case, the strains due to axial force and bending are zero. The principal strains from torsion, $\epsilon_{①}$ and $\epsilon_{②}$, occur on angles of 45° from the z-axis. Construction of Mohr's Circle shows that the axially located gages undergo no strain.

$$\epsilon_{g3} = \epsilon_{g6} = \epsilon_{g9} = \epsilon_{g12} = \epsilon_{①} = \epsilon_{②} = 0$$

Substitution into equation (3D),

$$\Delta e = c\ (0+0) = 0$$

shows that a twisting moment causes no change in the bridge output.

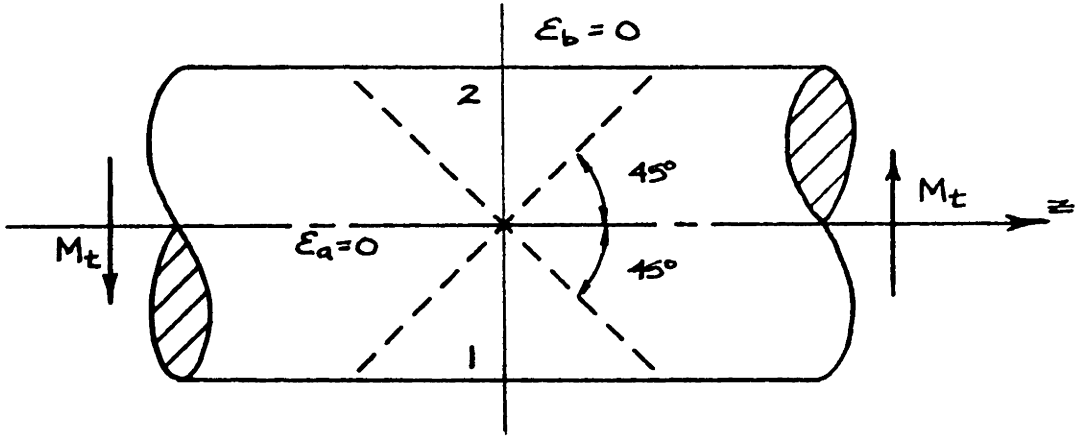

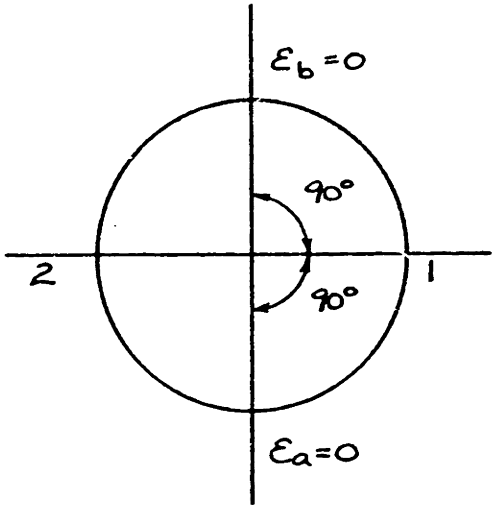

M_t = Twisting Moment

$\epsilon_{①}$ & $\epsilon_{②}$ = Principle Strains

ϵ_a & ϵ_b = Axial and Circumferential Strains

Figure 3.15

Independence of Torsional Loads

The bridge could be compensated for temperature variations by placing dummy gages in arms 2 and 4 of the bridge. These gages are placed on non-loading surface. If the temperature shifts uniformly throughout the load cell, the resistance of the gages in each arm will change by an identical amount:

$$(3E) \qquad \frac{\Delta R_1}{R_1} = \frac{\Delta R_2}{R_2} = \frac{\Delta R_3}{R_3} = \frac{\Delta R_4}{R_4}$$

Substitution into (3A) yields:

$$\Delta e = C\left(\frac{\Delta R}{R} - \frac{\Delta R}{R} + \frac{\Delta R}{R} - \frac{\Delta R}{R}\right) = 0$$

If the temperature variations in the load cell are not uniform, equation (3E) is not satisfied and the bridge will not be compensated. However, the main application of this load cell is for dynamic conditions, where the strains vary rapidly relative to temperature. Temperature compensation is not overly important, so no dummy gages were used.

Gages 1, 5, 7, and 11 and gages 2, 4, 8, and 10 measure the shear force in the x- and y- directions, respectively. The gages are arranged in adjacent arms of the bridges as in Figure 3.16.

According to Timoshenko (19), the strain in the column

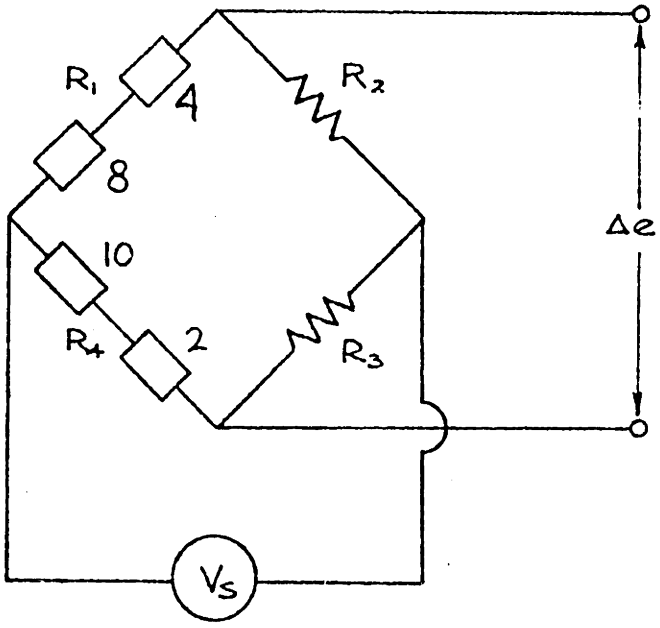

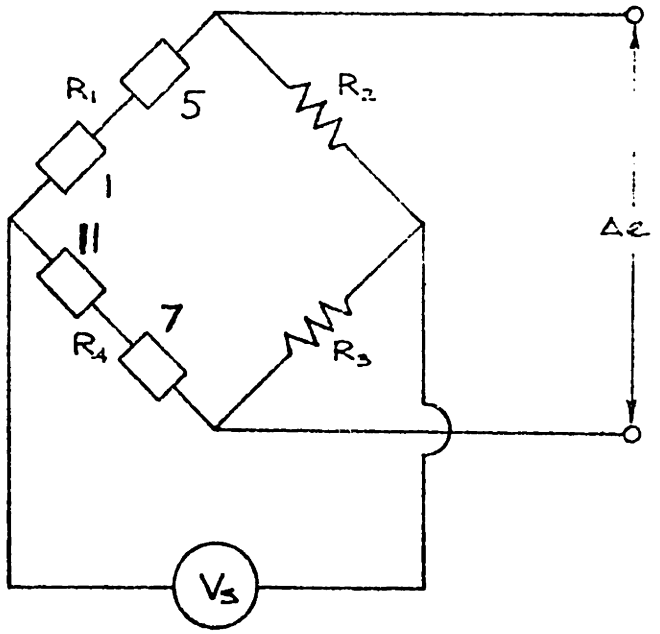

Figure 3.16

Bridge Configurations for Measurement of Shear Forces

is proportional to the applied shear force S.

$$\epsilon = \frac{S\ (b/2)}{4\ (b^4/12)E}$$

The gages on opposite sides of a column will be subjected to strains of equal magnitude but opposite sign such that for x-direction shear:

$$\epsilon_{g1} = -\epsilon_{g11} \quad \text{and} \quad \epsilon_{g5} = -\epsilon_{g7}$$

Substitution of these values into (3D) gives the bridge output.

$$\Delta e = c\left[(\epsilon_{g1} + \epsilon_{g5}) - (-\epsilon_{g1} - \epsilon_{g5})\right] = 2c(\epsilon_{g1} + \epsilon_{g5})$$

The circuit adds the strains due to shear from two identical columns on opposite sides of the load cell. The output is four times the average response of a single 120 ohm gage.

The bridge output is independent of axial force. Two gages on the same column will be subjected to the same axial strain:

$$\epsilon_{g1} = \epsilon_{g11} \quad \text{and} \quad \epsilon_{g5} = \epsilon_{g7}$$

Substituting into equation (3D), the output is unaffected.

$$\Delta e = c\left[(\epsilon_{g1} + \epsilon_{g5}) - (\epsilon_{g1} + \epsilon_{g5})\right] = 0$$

The output is also independent of temperature for uniform variations within each column. Strain gages on opposite sides of each column will undergo identical changes in resistance.

$$\frac{\Delta R_{g1}}{R_{g1}} = \frac{\Delta R_{g11}}{R_{g11}} \quad \text{and} \quad \frac{\Delta R_{g5}}{R_{g5}} = \frac{\Delta R_{g7}}{R_{g7}}$$

Substitution into equation (3C) yields:

$$\Delta e = C\left[\left(\frac{\Delta R_{g1}}{R_{g1}} + \frac{\Delta R_{g5}}{R_{g5}}\right) - \left(\frac{\Delta R_{g1}}{R_{g1}} + \frac{\Delta R_{g5}}{R_{g5}}\right)\right] = 0$$

If the variations are not uniform, the circuit will not be temperature compensated. As before, however, this is not critical in dynamic measurement.

In the same way as before, the bridge is also independent of torsion. The same analysis as above holds true for the y-direction shear forces.

3.4 Other Components of Force System

Due to manufacturer's tolerances, the resistances in the bridge arms are not all equal and a balancing circuit is required, as shown in Figure 3.17. The overall resistance of the zero-balancing circuit must be

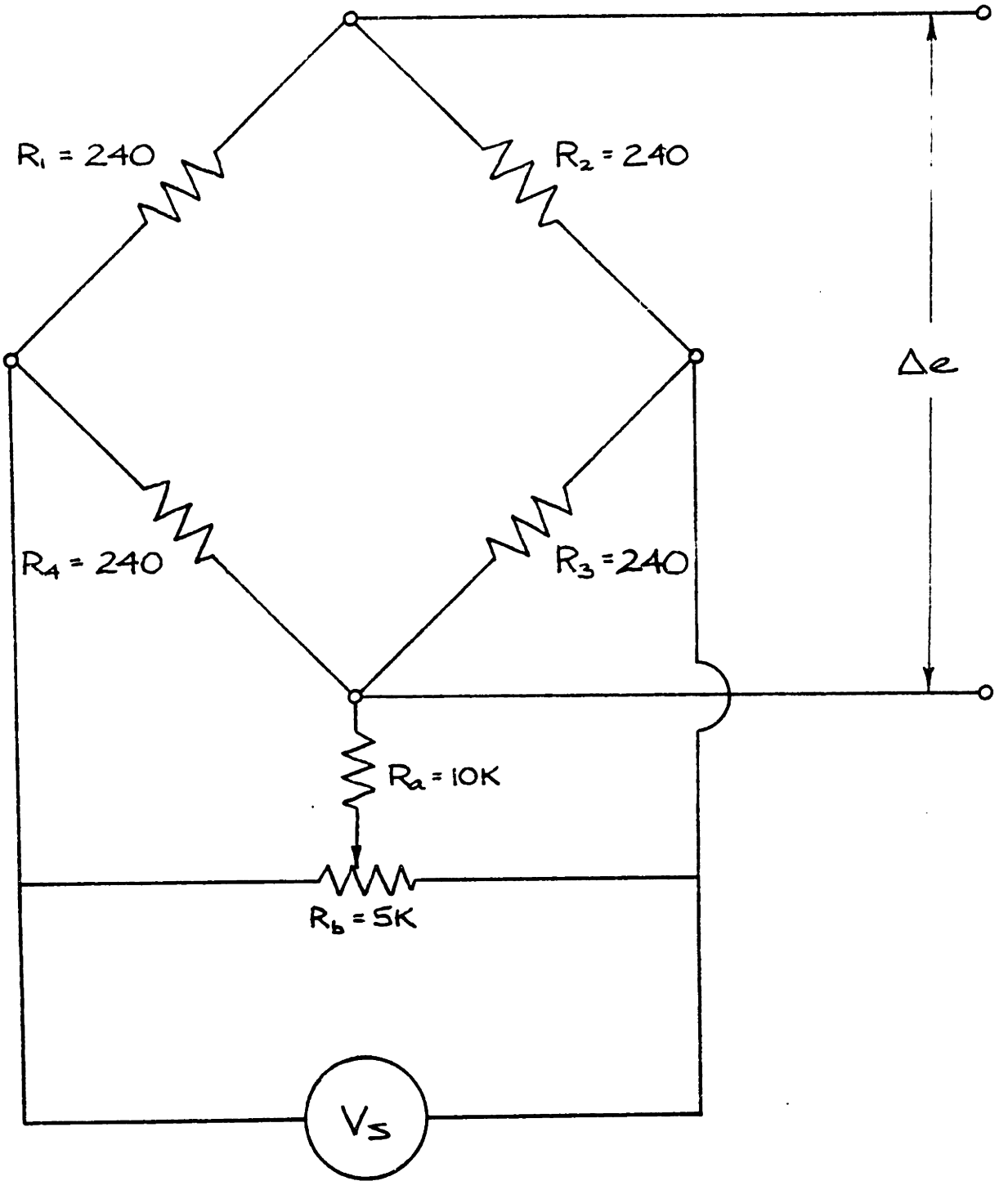

Figure 3.17

Wheatstone Bridge Balancing Circuit

variable over a range at least equal to the maximum possible initial unbalance of the bridge. The required range can be expressed by:

$$r_o = \sum_N 2p$$

where:

p_N = unit tolerance of resistance in Nth arm of bridge

For two 240 ohm resistors with tolerances of ±5% and four 120 ohm gages with tolerances of ±.2 ohms, this range is 49 ohms. Resistors should be used with a value of 240 ± 2 ohms to reduce the range to 10 ohms. This also causes a decrease in the desensitivity factor, which indicates how much sensitivity the balancing circuit is taking away from the Wheatstone Bridge. From tables in Murray (13), it is determined that if R = 10,000 ohms and R is a 5000 ohm potentiometer, the circuit will have a range of 10 ohms and a de-sensitivity factor of 1%.

Strain gages are limited in their current carrying capacity by their ability to dissipate the heat generated. The capacity of the gages used is 25-50 mA, corresponding to a source voltage of 6-12 volts. It is advantageous to have a higher source voltage for greater sensitivity of the load cell. However, since the calibration of the load cell will be nearly static, thermal drift must be minimized. Therefore, a D.C. voltage of 5 volts will be supplied to the circuit.

The constant for the bridge circuit equations can now be determined:

$$C = V_S \frac{R_1 R_3}{(R_1+R_2)(R_3+R_4)} \cdot GF = (5 \text{ Volts})(.25)(2.03) = 2.54$$

Using equations (3A) and (3B), the sensitivity for the circuit can be calculated. The bridge output is 7.8 μV/lb. for axial forces and is 21.3 μV/lb. for shear forces. Interference noise makes a signal of this size extremely difficult to sense. The signal must be conditioned to allow its accurate recording. The output must pass through an amplifier such as the one shown in Figure 3.18. This is a variable gain differential amplifier requiring a power supply of ± 5 volts. The gain of the amplifier is controlled by the feedback resistor:

$$\frac{Vout}{Vin} = K = \frac{R_f}{R_i}$$

Where:

Vout = amplifier output voltage
Vin = input differential voltage
K = amplifier gain
R_f = feedback resistor
R_i = input resistor

The maximum gain for the amplifier shown is 100.

Much of the noise present can be filtered out, since the highest frequency component in walking is only about 500 hertz. The RC low pass filter in Figure 3.19 has a cutoff

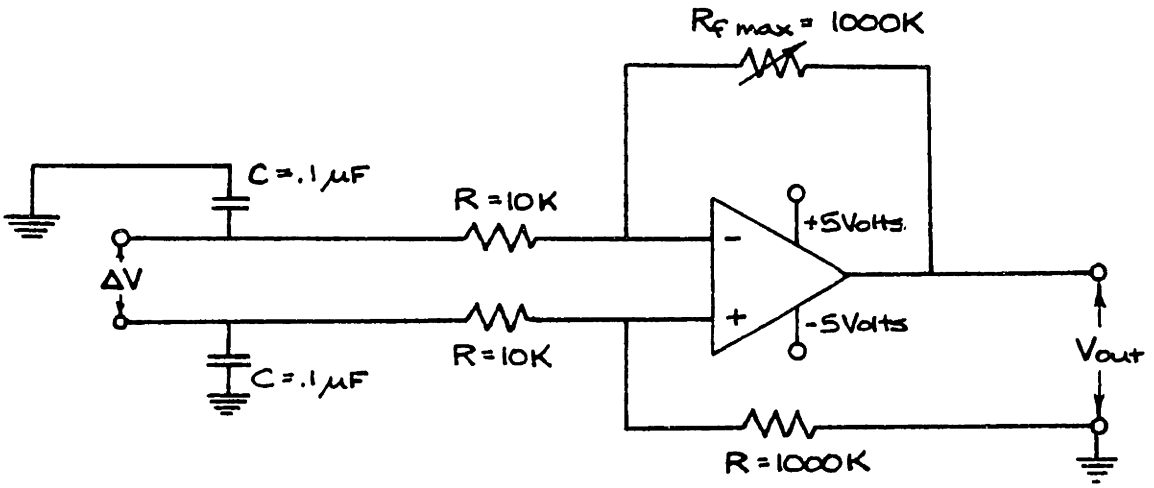

Figure 3.18 Differential Amplifier

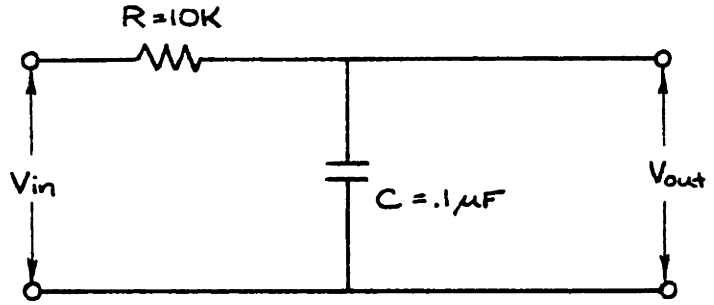

Figure 3.19 RC Lowpass Filter

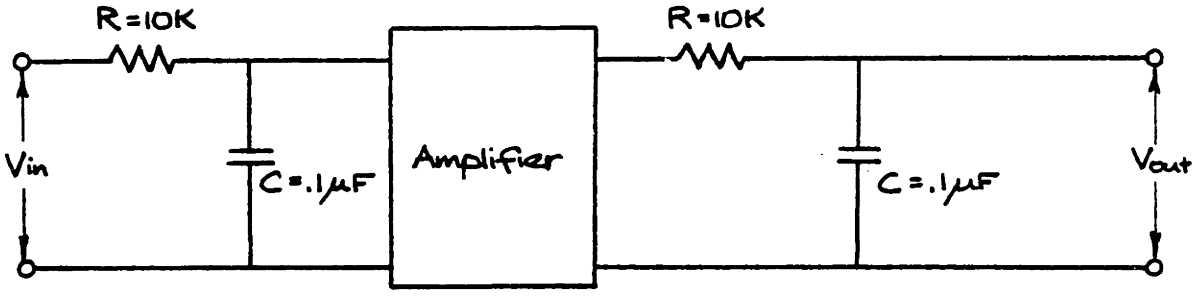

Figure 3.20 Non-loading Cascaded RC Lowpass Filter

frequency of 1000 hertz. However, for first order systems the attenuation is quite gradual. Cascaded elements provide a sharper cutoff. Ogata (14) recommends inserting the amplifier between the stages as in Figure 3.20. The high input impedance amplifier effectively unloads the two circuits to prevent an undesired loss of gain by the filters due to loading effects.

The analog output of the filters should be digitized in an analog to digital converter (ADC). The digital signals will be sampled and recorded for later processing by a computer. A schematic of the entire proposed system is shown in Figure 3.21. A wiring diagram for a single load cell is shown in Figure 3.22.

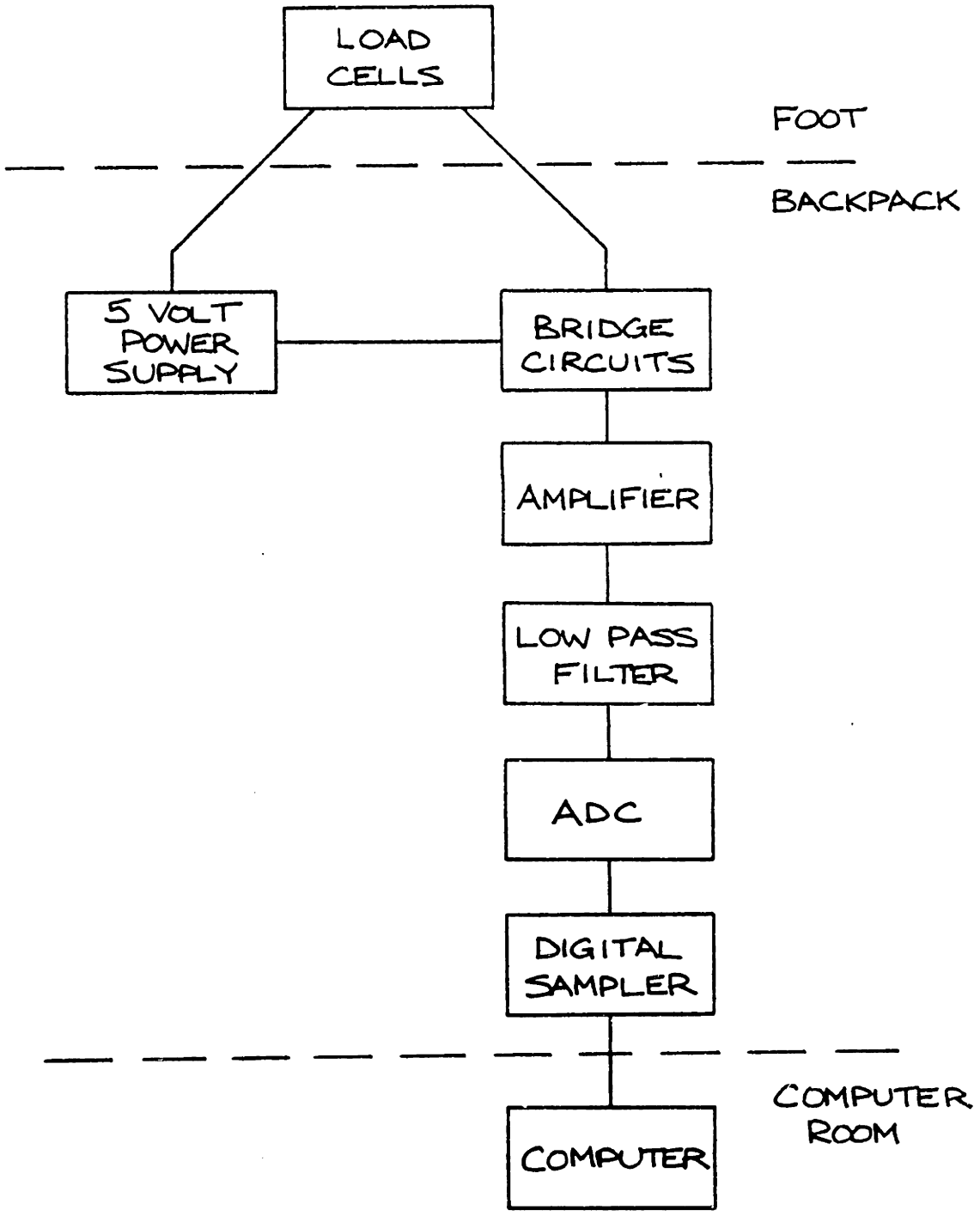

Figure 3.21

Proposed Force Measuring System

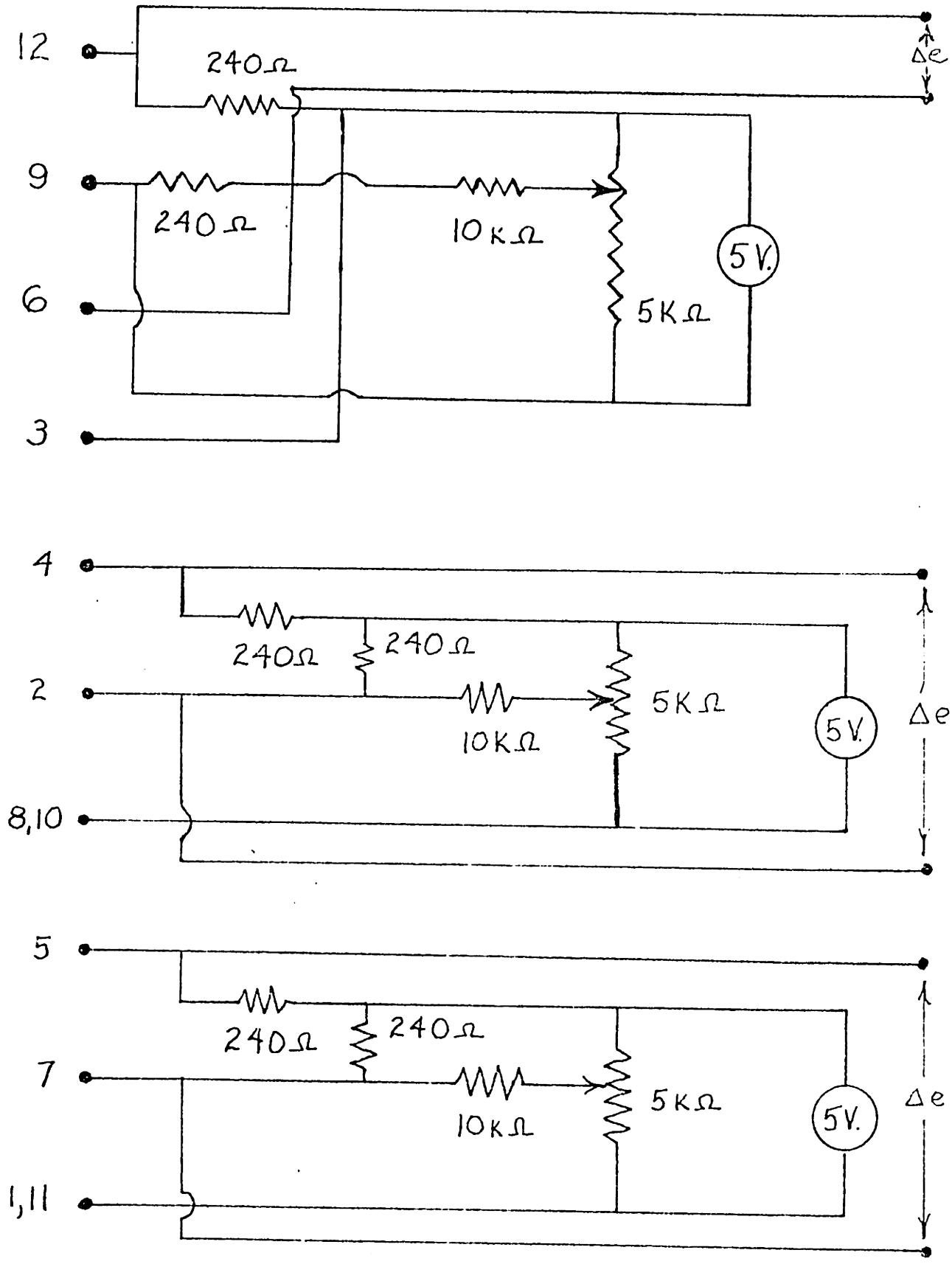

Figure 3.22

Load Cell Wiring Diagram

CHAPTER 4: CONSTRUCTION AND TESTING OF LOAD CELL

4.1 Construction

The load cell was made out of a single block of 2024 aluminum on a milling machine. The quality of machining was reasonable. The dimensions of the column sides ranged from .175 inches to .181 inches.

The gages were mounted on the columns with a high quality transducer adhesive, QA-550 from BLH Electronics. The gages were positioned with lines located .15 inches from the mounting plate edge and along the center of each column. A 4x magnifying glass was required for accurate placement of the gages. Nevertheless, slight misaligment occured in all of the gage placements. The gages and leads were mechanically protected and electrically isolated by a coating of RTV silicone rubber.

It was found that the available terminal loops would not fit on the load cell as planned. The size of the terminals forced the construction of a plastic cover for their placement. Another plastic cover was made to fit over the terminals and to protect the axial force gages on the outside of the load cell. These covers are shown in Figure 4.1. The covers are much bigger than desired for actual use

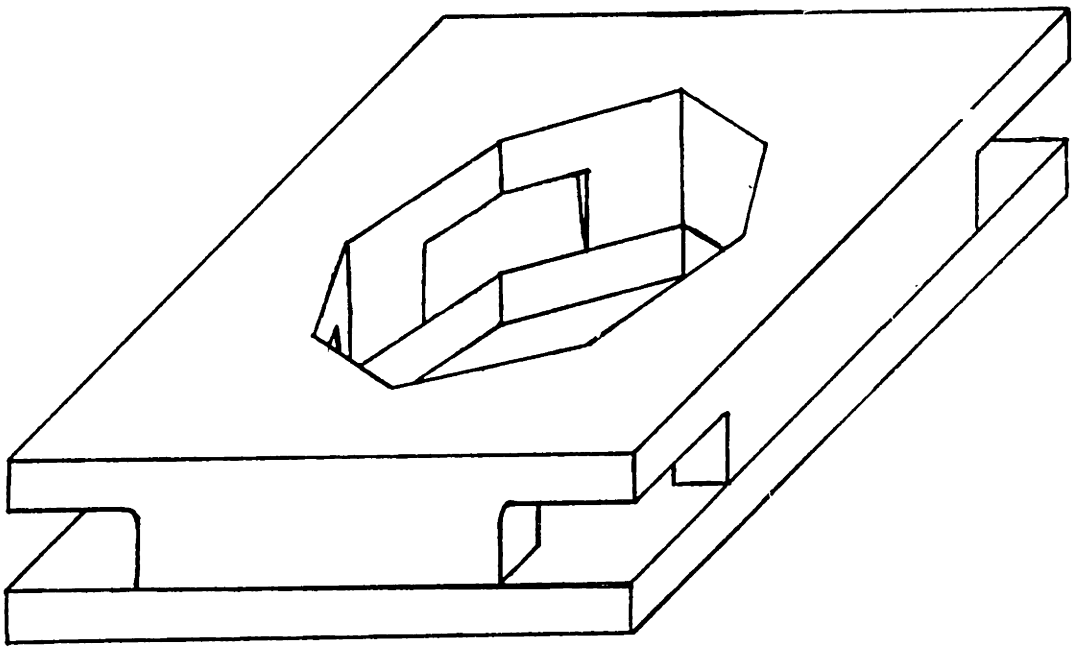

Figure 4.]

Constructed Load Cell Covers

of the load cell, but are acceptable for use with this prototype. The weight of the load cell was about .03 pounds. The complete load cell is shown in Figure 4.2.

4.2 Testing Procedure

For testing, the bridge circuit power was supplied by a 5 volt D.C. rectifier supplied by the line voltage. Quality electronic equipment was used to ensure that all problems will actually be in the load cell and not in the electronics.

Preliminary testing on the device was performed by placing known weights on top of the load cell. The bridge outputs were fed to a Tektronix 7613 oscilloscope. The output was processed by a type 7A22 differential amplifier, which contained a one kilohertz low-pass filter. The lowest gain setting was 100μV/cm, giving a resolution of 10μV for the scope. The load cell gave consistent readings of 8-9 μV/lb. The resolution was about 2 pounds. The noise was on the order of 40 μV. D.C. drift ranged from 10-30 μV/minute, an insignificant amount. When the voltage supply was increased to 15 volts, the drift was too large for the load cell to remain functional.

To obtain more accurate calibration, the load cell was tested on a Model 1125 Instron. The Instron is accurate to within 1%. A 1000 pound compression load cell was used.

The foot load cell was strained at a rate of .002 inches per minute. The Instron plots on chart paper a force versus time curve. The foot load cell was calibrated by recording the oscilloscope reading at fixed time intervals of ten seconds and plotting this value against the corresponding Instron load at that time. The Instron full load scale was 200 lbs. for axial forces and 100 lbs. in the shear mode. These low values were chosen to ensure that the load cell did not yield and to obtain more accurate readings of the Instron forces. A Tektronix D13 ascilloscope with a 5A2ON Differential Amplifier was used for this test. The maximum gain for this amplifer is one fifth of the gain of the 7A22. The resolution of reading data off the scope dropped to 50μV.

The load cell was tested in a number of different ways. Five runs were made of a simple uniaxial compression test, shown in Figure 4.3. Runs 6-8 measured the force from a 3/8 inch diameter washer, centered 1/4 inch from the center of the load cell, as shown in Figure 4.4. In runs 9 and 10, the load was applied to one half of the surface area of the load cell, as shown in Figure 4.5. Runs 11-15 tested the load cell in the shear mode. In runs 11-13, the shear load was applied directly to the load cell as seen in Figure 4.6, clamped at the bottom and unrestrained at the top. In runs 14 and 15, the top plate of the load cell was clamped to the block, as in Figure 4.7, to measure the effect

Figure 4.2

Completed Load Cell

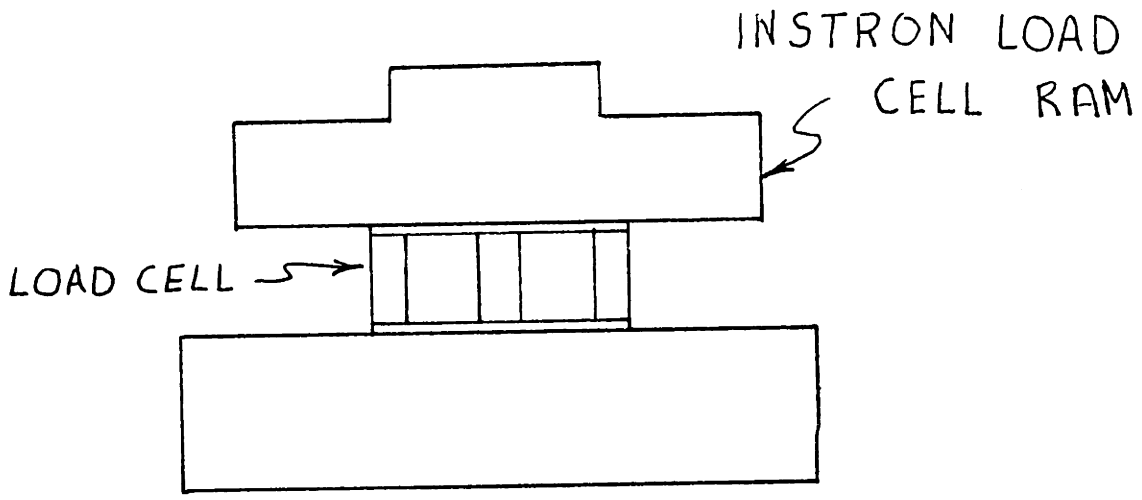

Figure 4.3: Instron Set-up for Uniform Axial Loading

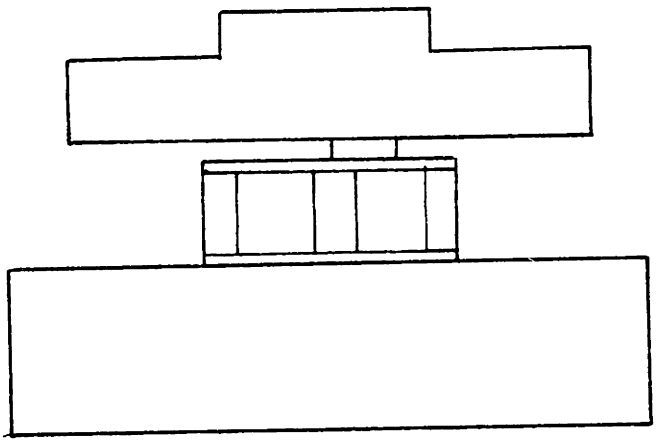

Figure 4.4: Instron Set-up for Axial Loading

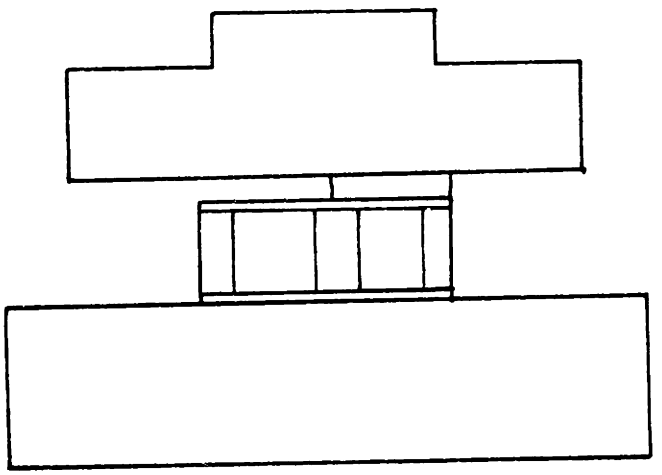

Figure 4.5: Instron Set-up for Axial Loading

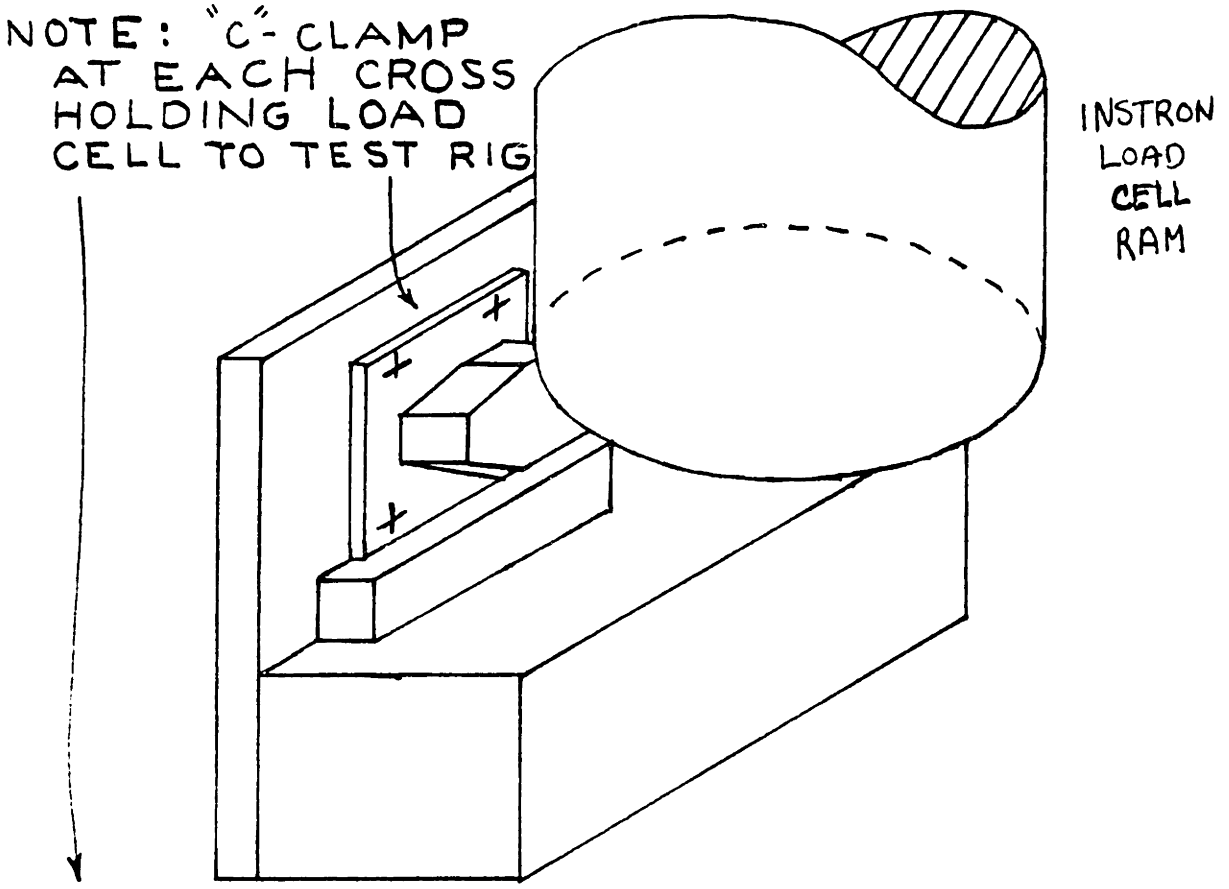

Figure 4.6: Instron Set-up for Shear Loading

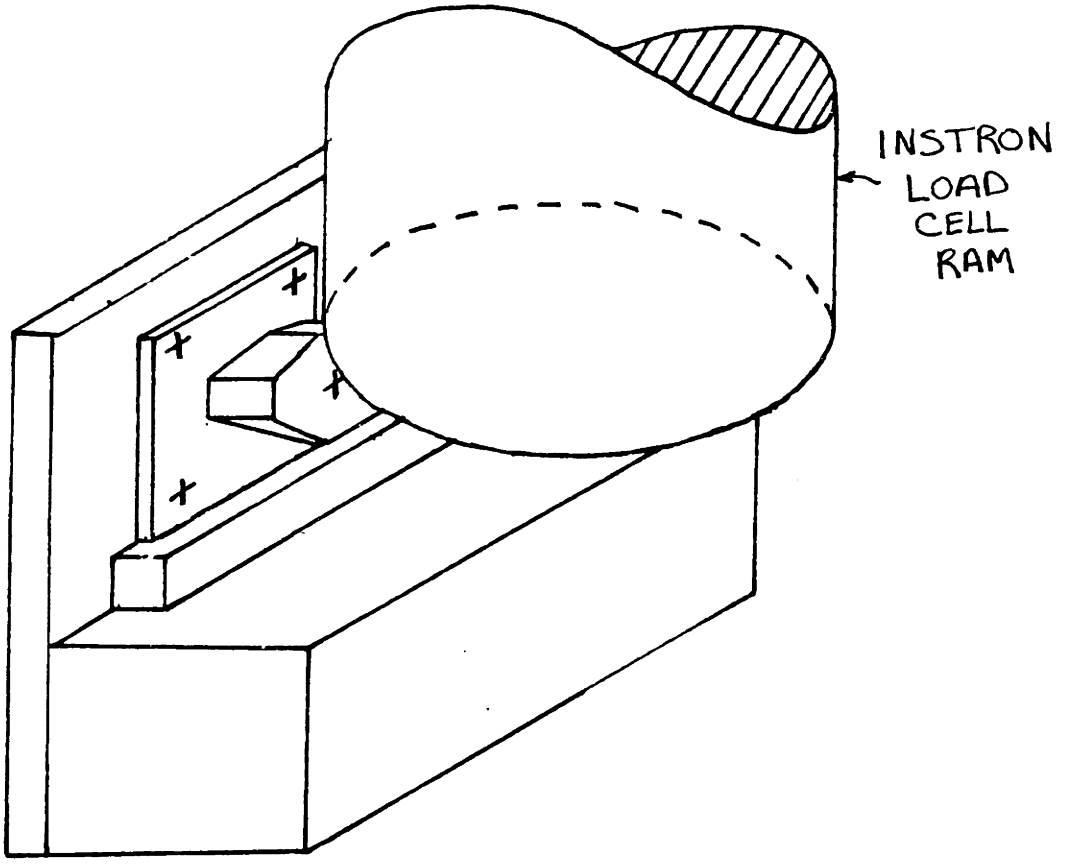

Figure 4.7: Instron Set-up for Combined Loading

of axial force on shear force output.

4.3 Results and Discussion

The calibration curves obtained were approximately linear. Table A.1 in Appendix A gives the data for the individual calibration runs along with the calculated sensitivity, linear correlation coefficient, and least squares fitted relationship. Calibration curves for individual curves are given in Figure A-1 through A-15. Appendix B shows how these values are determined.

The scatter diagram and least squares best fit for the five runs in uniform axial loading is shown in Figure 4.8. The correlation coefficient for this curve is .990, the greatest for all the loading modes attempted. The sensitivity for any one run was within 9% of the combined sensitivity of 9.7μV/lb. This compares with a theoretical value of 7.8μV/lb for columns .18 inches thick.

The calibration curves for runs 6 through 8 is shown in Figure 4.9. The sensitivity dropped down to 3.95μV/lb and the curve exhibited the least linearity of all types of loading tested. In runs 7 and 8, the bridge output went negative before rising. This data might be explained by the fact that the load is applied over a small, unsupported portion of the endplate. The plate loses its rigidity and deflects downward, bending the columns inward and causing a

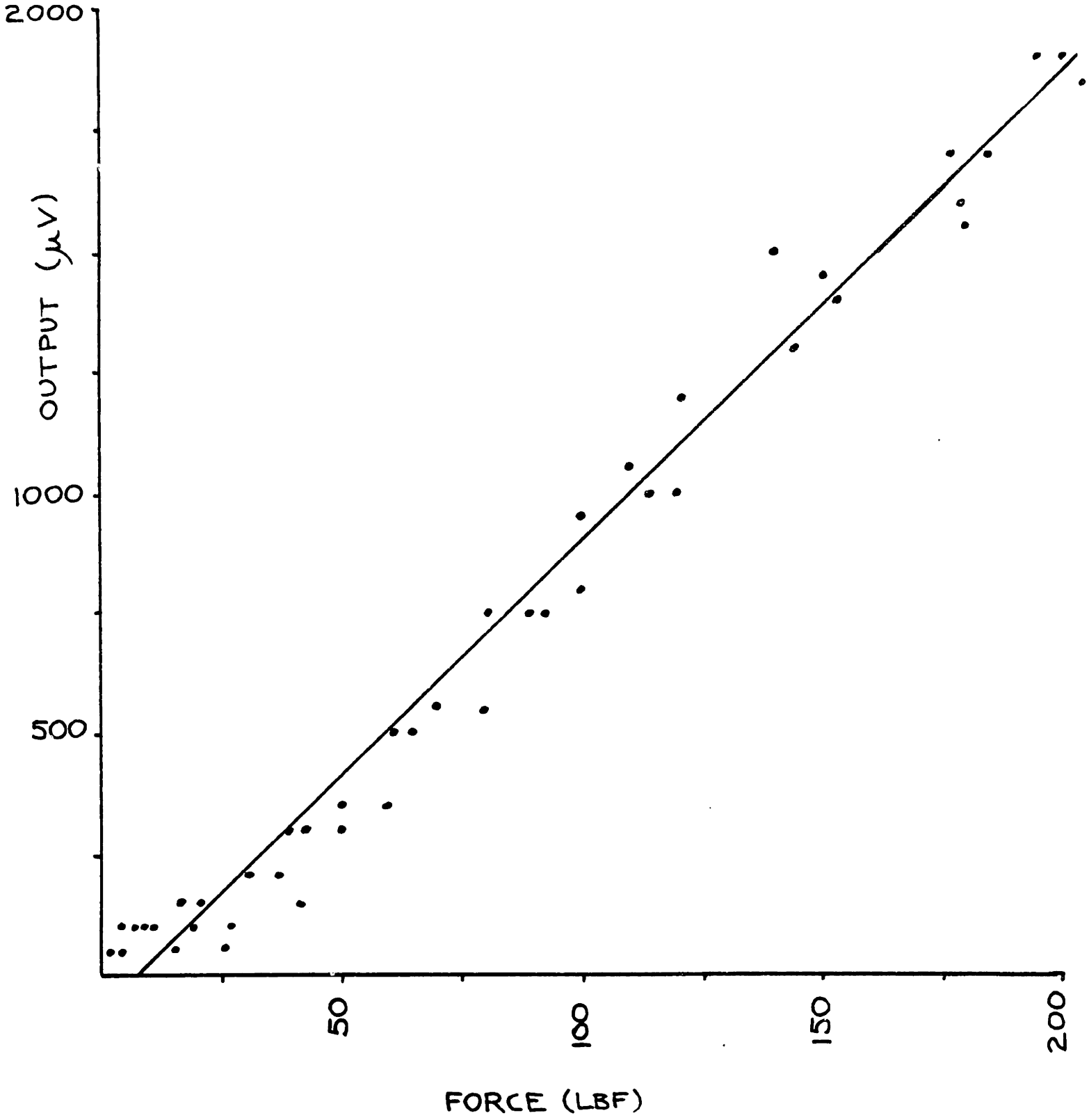

Figure 4.8

Calibration Curve for Uniform Axial Loading Runs 1-5

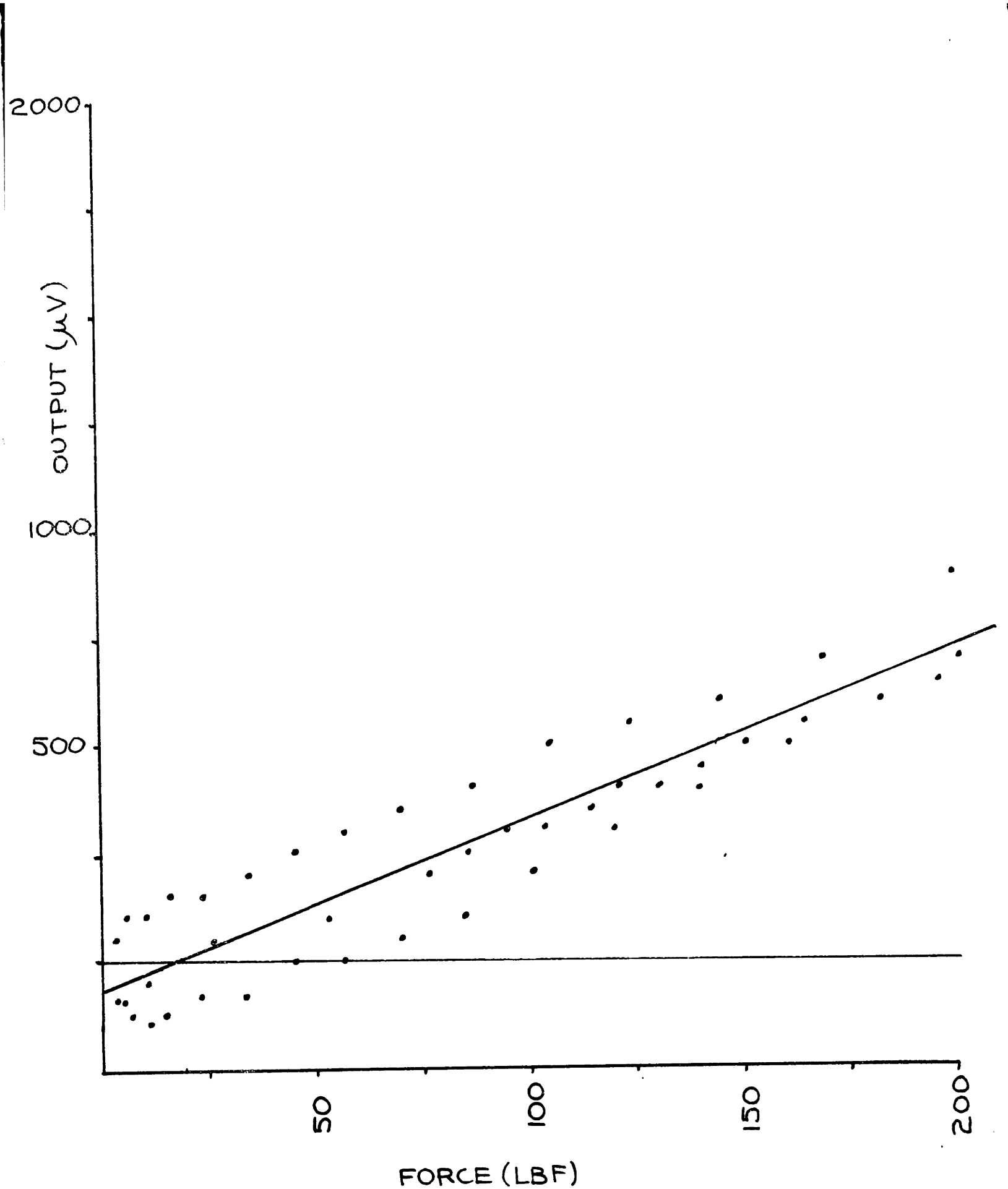

Figure 4.9

Calibration Curve for Off-center Axial Loading Runs 6-8

negative output. As the force increases, both inward bending and axial compression of the columns occurs. These two effects are opposite in sign and cancel out much of the output.

The validity of this argument is supported by the results of calibration runs 9 and 10, shown in Figure 4.10. When the load is applied over one-half of the load cell surface, the sensitivity of 8.3 μV/lb approaches the value for the uniformly loaded case.

The calibration curve for shear loading in Figure 4.11 has a sensitivity of 9.1 μV/lb. Run 11 had a sensitivity about 20% higher than for the other two runs, indicating that the load cell was more tightly clamped at first but slipped in subsequent runs.

An axial force was applied in Runs 14 and 15, clamping the load cell much better. As a result of the increased rigidity of the system, the sensitivity increased to 10.4 μV/lb for the graph in Figure 4.12. The theoretical sensitivity for shear loading is much higher at 21.3 μV/lb.

Table 4.1 summarizes the data for the different loading modes tested. The accuracy and linearity of the data is limited by the system resolution of about five pounds for most runs. Increased amplification is desired.

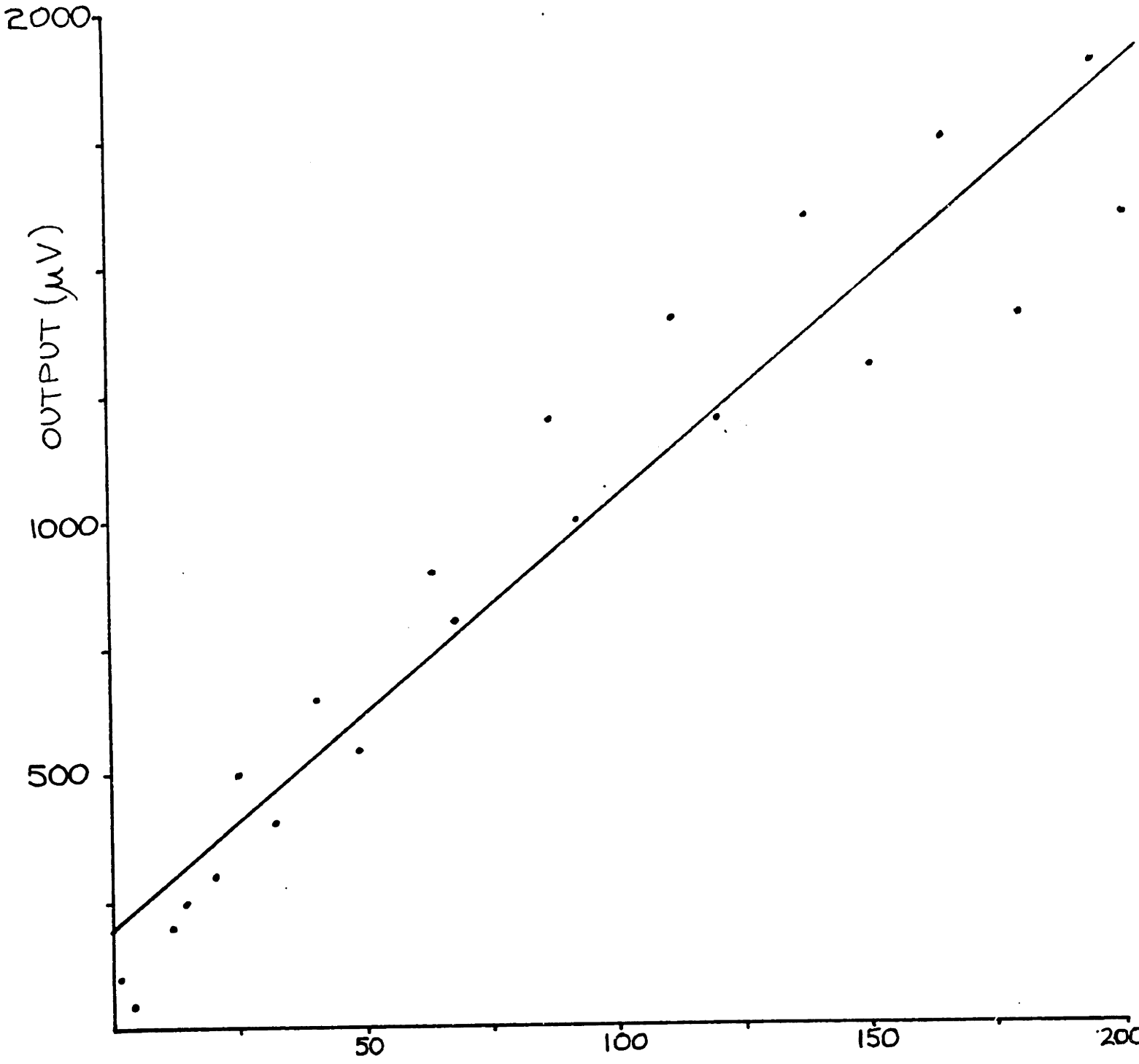

Figure 4.10

Calibration Curve for Axial Loading On One-half of Load Cell Runs 9-

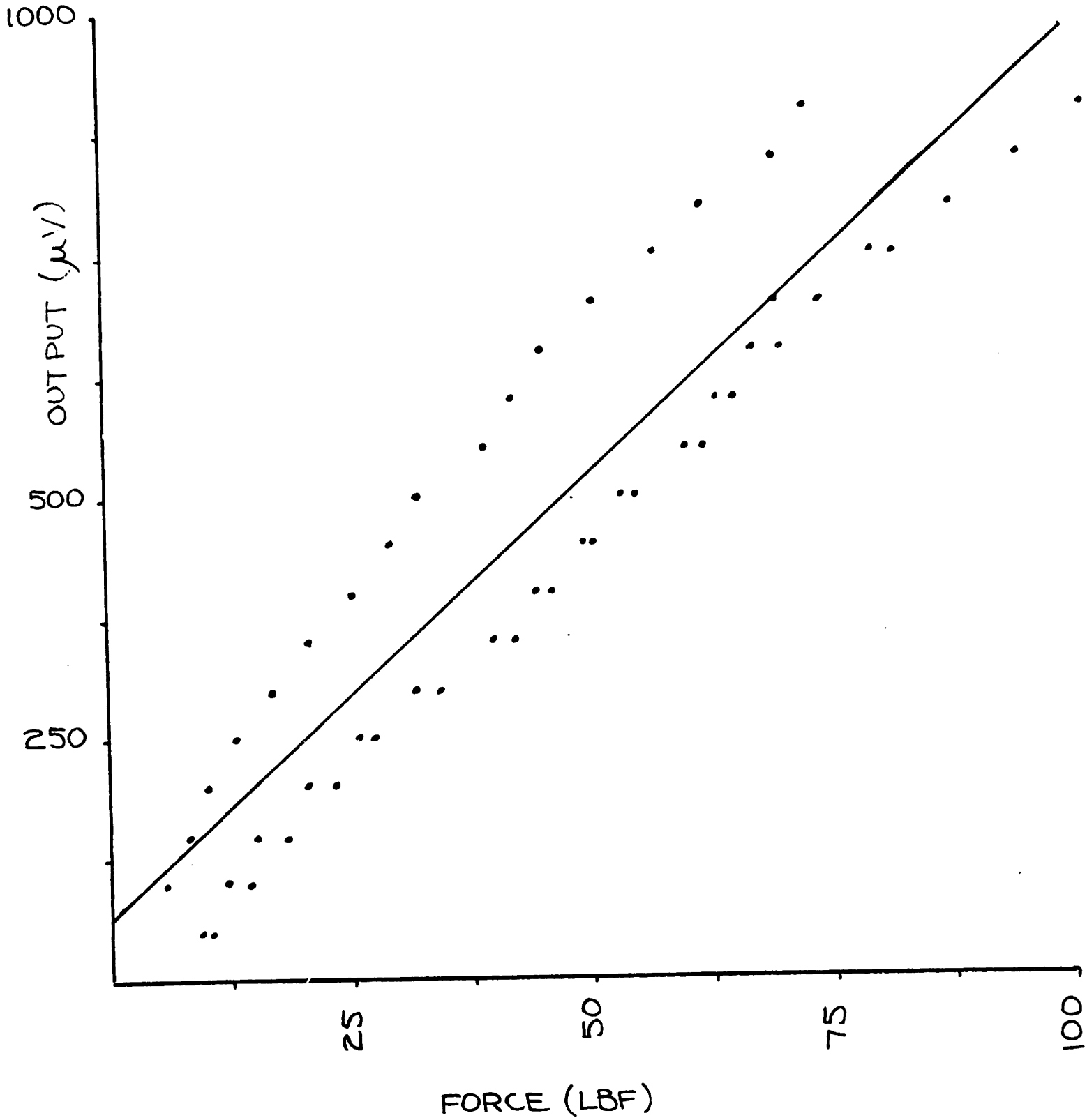

Figure 4.11

Calibration Curve for Shear Loading Runs 11-13

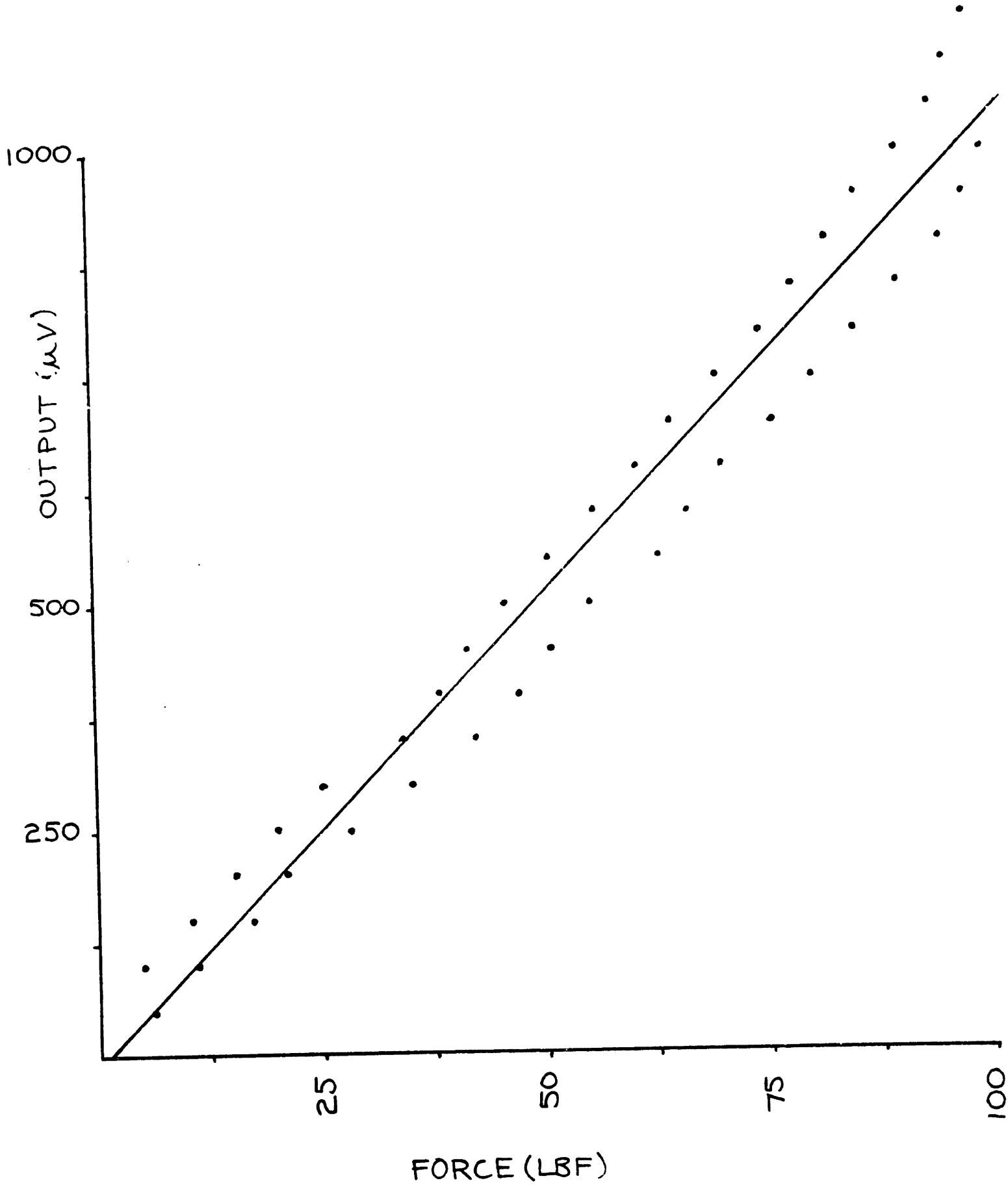

Figure 4.12

Calibration Curve for Shear Loading with Axial Force Runs 14-15

Table 4.1

Run Nos.	Loading	m	V	x	y
1-5	Uniform-Axial	9.68	.990	7.8	-75.5
6-8	Off-Center-Axial	3.95	.921	19.2	-76.0
9-10	Half of Surface Axial	8.34	.958	-24.0	200.6
11-13	Shear	9.11	.926	-6.7	61.3
14-15	Shear with Axial	10.43	.981	1.0	110.5

where: m = sensitivity (μV/lb)
r = linear correlation coefficient
x_{int} = interception of force axis by line (lbf)
y_{int} = interception of output axis by line (μV)

The results of runs 6 through 8 shows the importance of reducing overhang for good results. In practice, the load cell will not be loaded in this manner, but the importance of edge effects is seen. The variation in output for shear loads demonstrates the importance of rigid mounting for accurate measurement.

CHAPTER 5: CONCLUSION

5.1 Evaluation of Present Design

The load cell built has a reasonable sensitivity over a wide range of loads in both the axial and shear modes. The load cell is approximately linear, with the greatest nonlinearities occuring for small loads. The resolution of the system tested is 5 pounds force, compared with the desired one pound force. With more amplification, this resolution could be reached. Machining of the load cell is not nearly as difficult as accurate placement of the strain gages and placement of all the leads inside the cell.

5.2 Recommendations

Some changes in the design details should be made. The axial gages on the outside of the load cell should be inverted so that the leads point downwards for better protection. The resistor in the fourth arm of the bridge should be placed in the load cell so that the signal does not have to leave the load cell, travel ten feet and return, thereby picking up a great deal of noise. Smaller terminals must be used to reduce the size of the plastic cover. The strain gages must be more accurately placed on the columns. It may be worthwhile to send the machined load cell out to a

transducer manufacturer for gage attachment. The electronics used must be carefully evaluated to ensure that load cell performance is not restricted.

Further experimentation is necessary under conditions that will simulate the actual use of the load cell. Mounting is critical as far as the static and dynamic characteristics of the transducer. The suggested mounting technique is impossible to assess without testing. Five of the load cells should be constructed and mounted on shoes in various manners to compare load cell performance under actual conditions.

APPENDIX A: DATA FOR INSTRON TESTING

Table A-1:
Symbols: r = linear correlation coefficient
m = sensitivity (μV/lb.)
b = y intercept
F = Instron applied force
V = bridge output

Run 1: Uniform Axial Loading
r = .9970
m = 10.48
b = 137.7

F	μV
15	50
18	100
27	100
37	200
50	300
63	500
80	750
99	950
121	1200
150	1450
176	1700
200	1900

Run 2: Uniform Axial Loading
r = .9966
m = 10.84
b = -266.

F	μV
26	50
41	150
59	350
79	550
100	800
116	1100
154	1400
184	1700

Run 3: Uniform Axial Loading
r = .9919
m = 9.17
b = -23.1

F	μV
1	50
3	100
6	100
16	150
30	200
49	300
70	550
92	750
120	1000
144	1300
178	1600
194	1900

Run 4: Uniform Axial Loading
r = .9919
m = 10.35
b = -47.9

F	μV
4	50
8	100
20	150
38	300
60	500
84	750
108	1050
140	1500

Run 5: Uniform Axial Loading
r = .9912
m = 9.19
b = -48.1

F	μV
5	50
10	100
22	150
42	250
65	500
88	750
113	1000
144	1300
175	1550
204	1850

Run 6: Off-center Point Loading
r = .9971
m = 3.82
b = -83.8

F	μV
0	- 100
4	- 100
10	- 50
17	0
27	50
40	100
53	100
65	150
76	200
86	250
95	300
104	300
114	350
122	400
132	400
141	450
151	500
169	550
178	600
196	650

Run 7: Off-center Point Loading
r = .9912
m = 9.19
b = -48.1

F	μV
4	- 100
6	- 150
11	- 200
17	- 150
24	- 100
34	- 100
45	0
57	0
70	50
85	100
102	200
120	300
141	400
162	500
183	600
202	700

Run 8: Off-center Point Loading
r = .9961
m = 3.97
b = 64.7

F	μV
3	50
5	100
10	100
16	150
24	150
34	200
45	250
57	300
70	350
86	400
105	500
124	550
145	600
168	700
199	900

Run 9: Half of Area Loading
r = .9824
m = 9.54
b = 211.1

F	μV
3	50
14	250
26	500
41	650
64	900
88	1200
112	1400
138	1600
166	1750
196	1900

Run 10: Half of Area Loading
r = .9859
m = 7.37
b = 180.9

F	μV
1	100
11	200
20	300
33	400
49	550
69	800
93	1000
121	1200
151	1300
181	1400
202	1600

Run 11: Shear Loading
r = .9936
m = 11.53
b = 93.8

F	μV
6	100
8	150
10	200
13	250
17	300
21	350
25	400
29	450
32	500
39	550
42	600
45	650
51	700
57	750
62	800
69	850
73	900

Run 12: Shear Loading
r = .9968
m = 9.85
b = -19.43

F	μV
9	50
12	100
15	150
21	200
26	250
32	300
40	350
44	400
49	450
53	500
60	550
63	600
67	650
69	700
79	750

Run 13: Shear Loading

r = .9987
m = 9.43
b = -25.0

F	μV
10	50
14	100
18	150
23	200
27.5	250
34	300
42	350
46	400
50	450
55	500
62	550
65	600
70	650
74	700
82	750
88	800
95	850
99	900

Run 14: Shear Output in Combined Loading

r = .9969
m = 10.99
b = 7.58

F	μV
6	50
11	100
17	150
21	200
28	250
35	300
42	350
47	400
51	450
55	500
63	550
66	600
70	650
76	700
80	750
85	800
89	850
94	900
97	950
99	1000

Run 15: Shear Output in Combined Loading

r = .9969
m = 9.85
b = -32.6

F	μV
6	50
11	100
17	150
21	200
28	250
35	300
42	350
47	400
51	450
55	500
63	550
66	600
70	650
76	700
80	750
85	800
89	850
94	900
97	950
99	1000

A-2 Calibration Curves for Instron Testing Runs

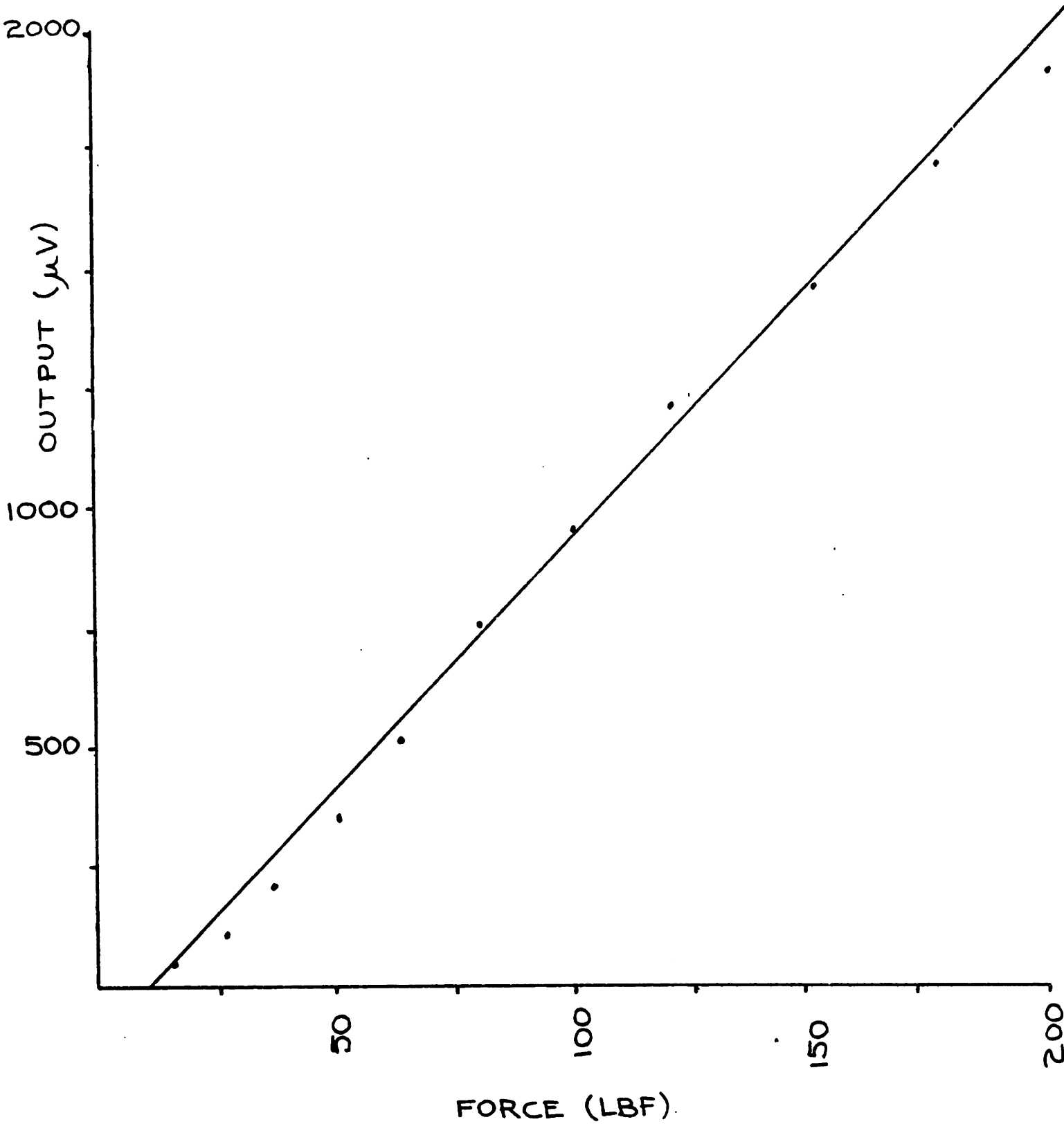

Figure A-1

Calibration Curve for Uniform Axial Loading Run 1

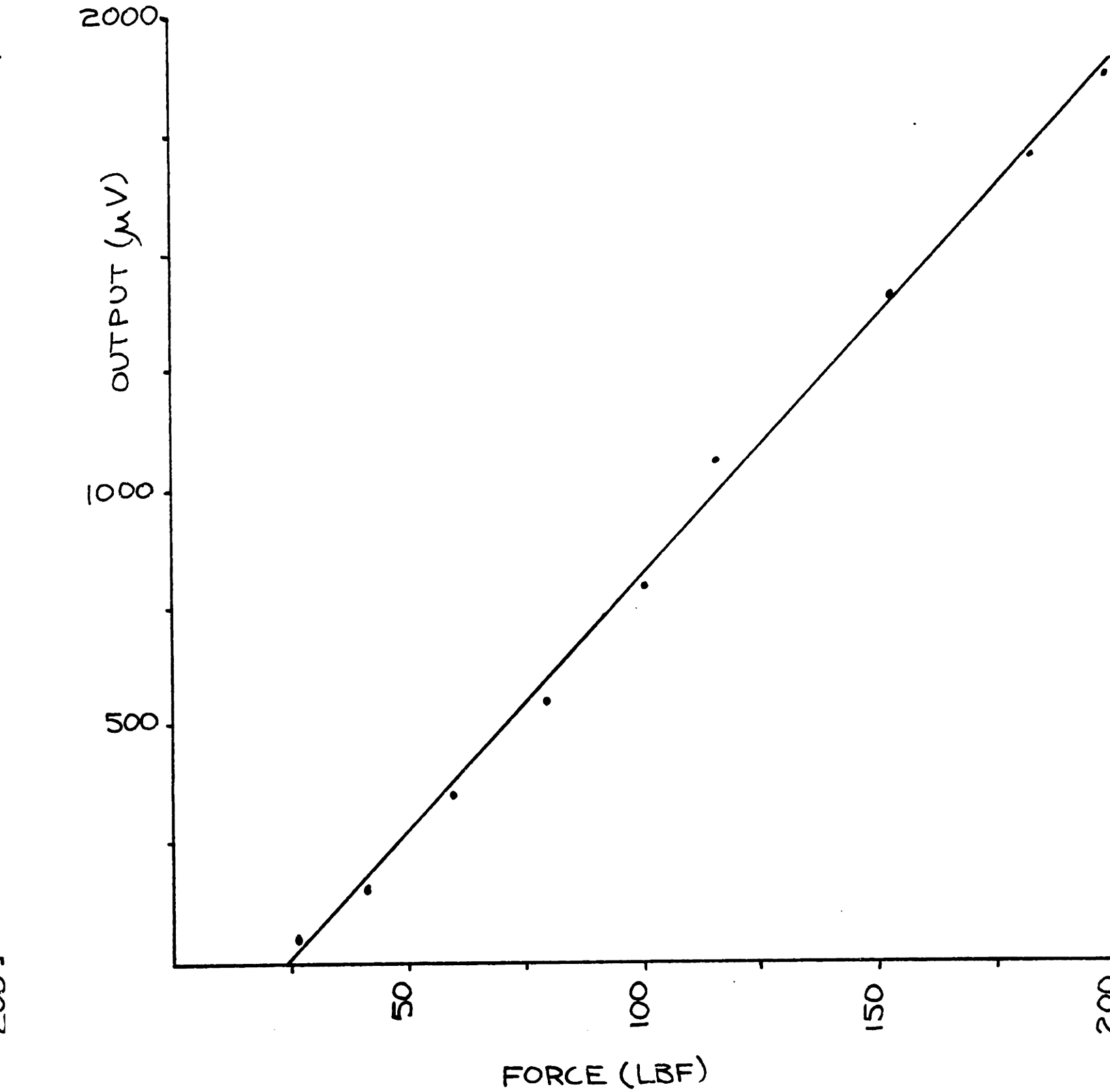

Figure A-2

Calibration Curve for Uniform Axial Loading - Run 2

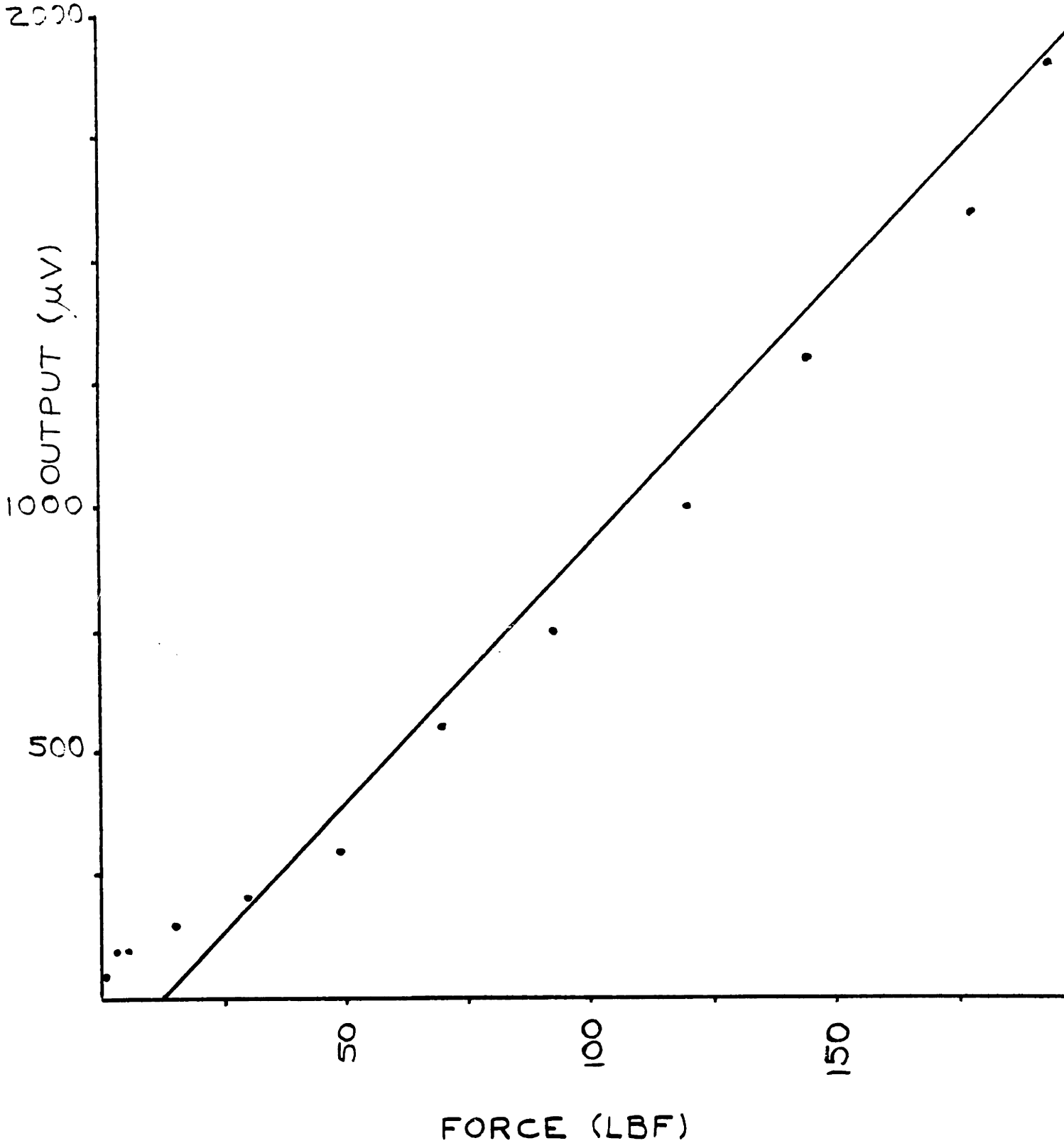

Figure A-3

Calibration Curve for Uniform Axial Loading - Run 3

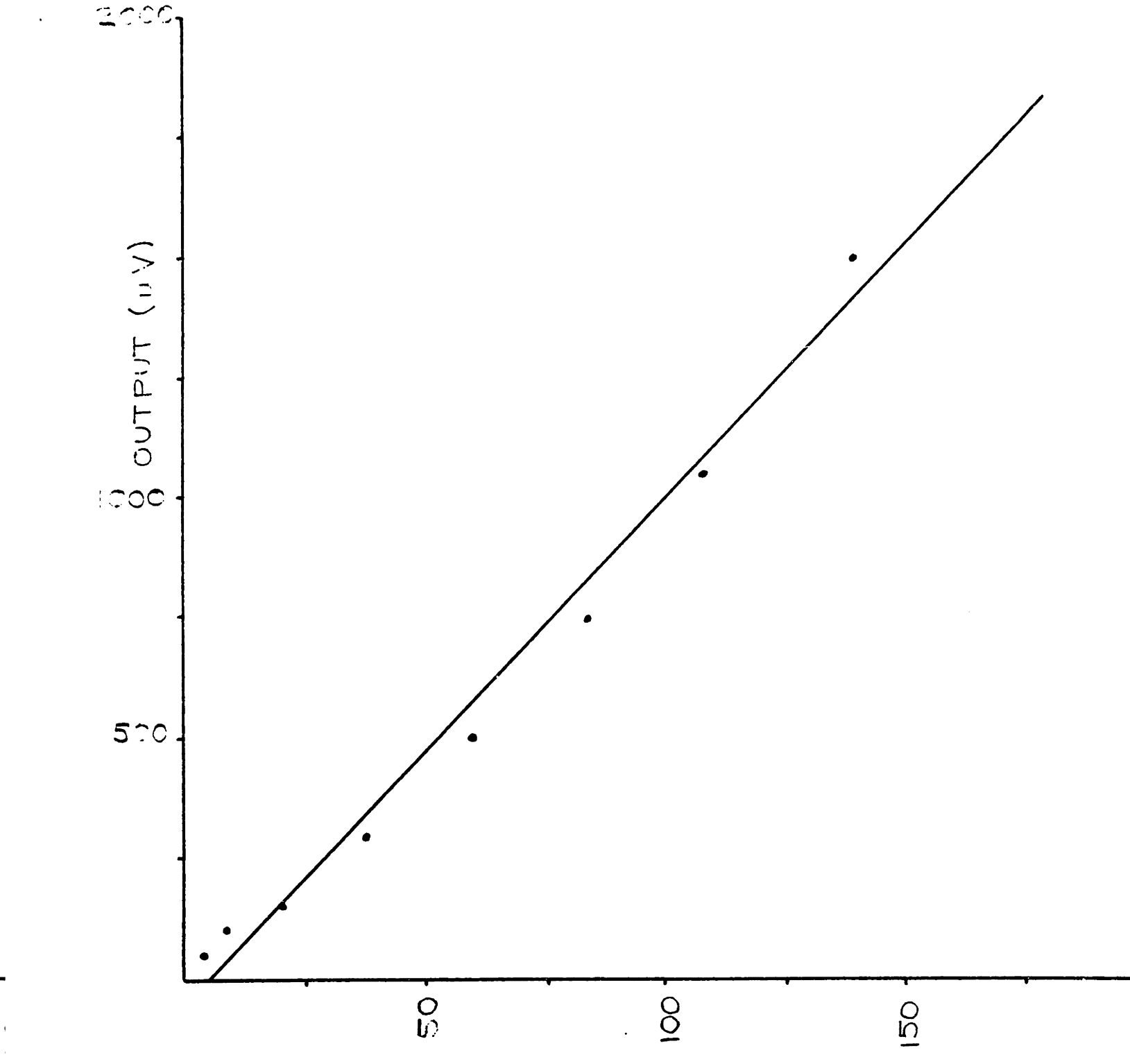

Figure A-4

Calibration Curve For Uniform Axial Loading - Run 4

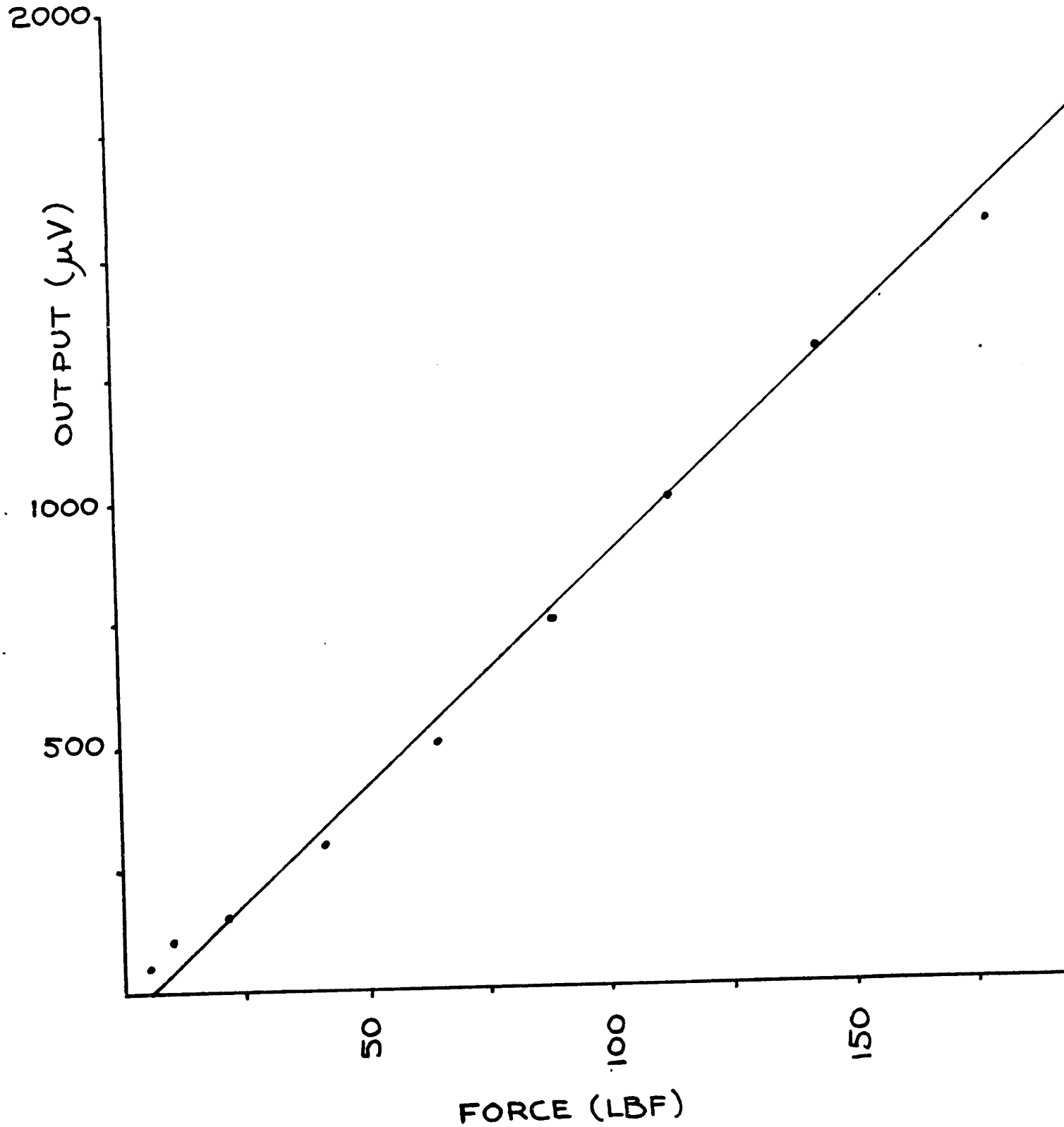

Figure A-5

Calibration Curve for Uniform Axial Loading - Run 5

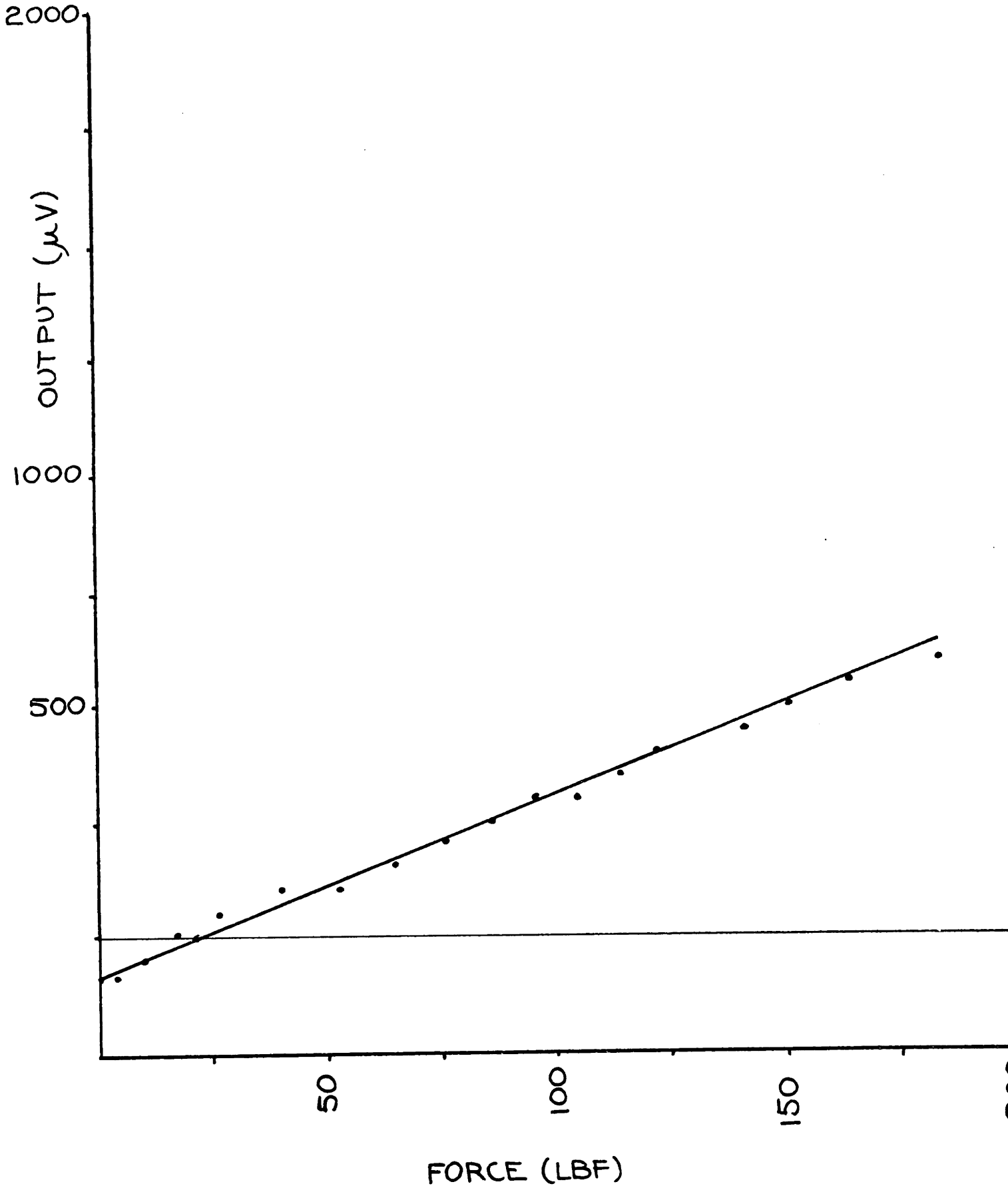

Figure A-6

Calibration Curve for Off-center Axial Loading - Run 6

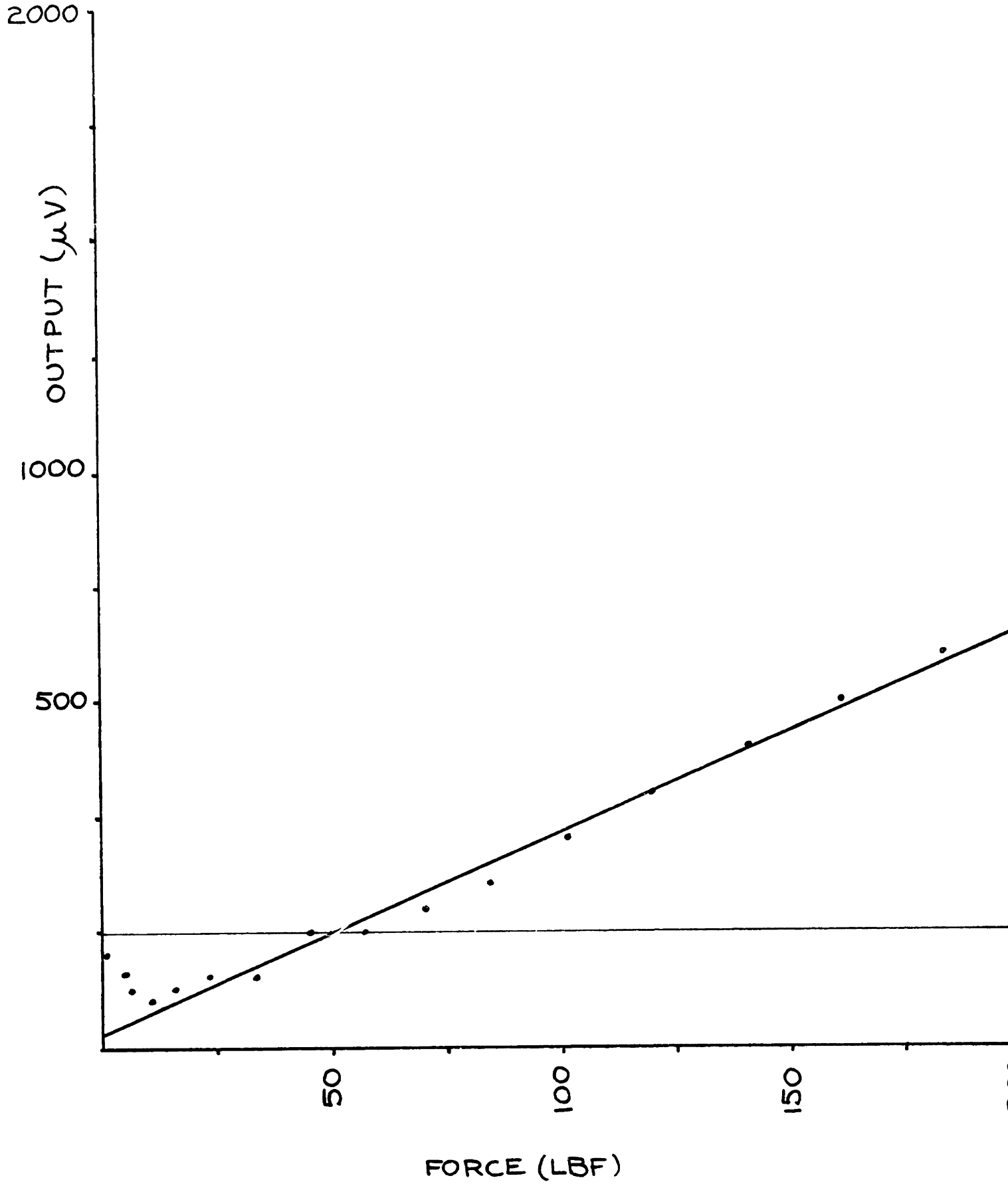

Figure A-7

Calibration Curve for Off-Center Axial Loading - Run 7

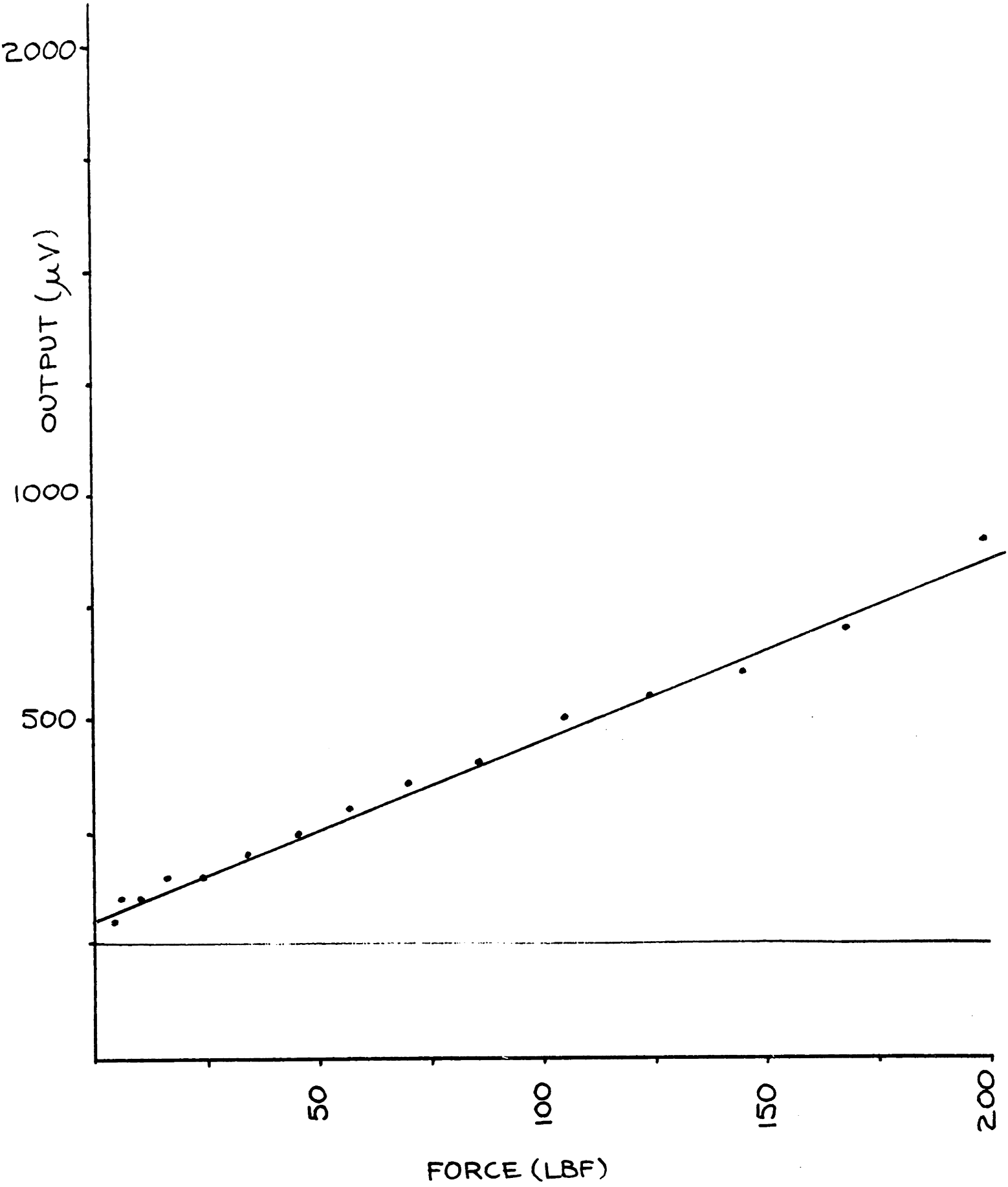

Figure A-8

Calibration Curve for Off-center Axial Loading - Run 8

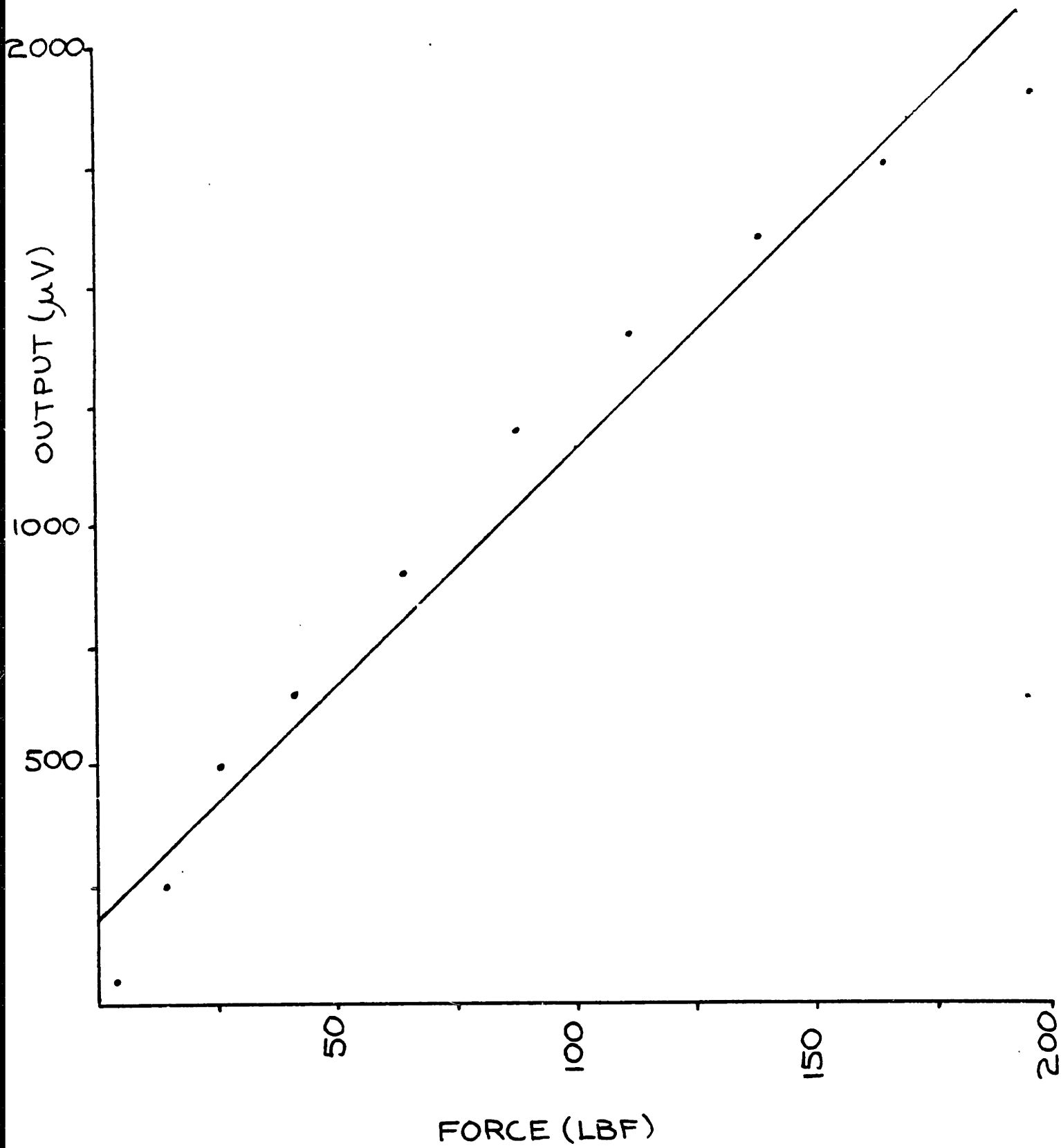

Figure A-9

Calibration Curve for Axial Loading on Half of Load Cell Run 9

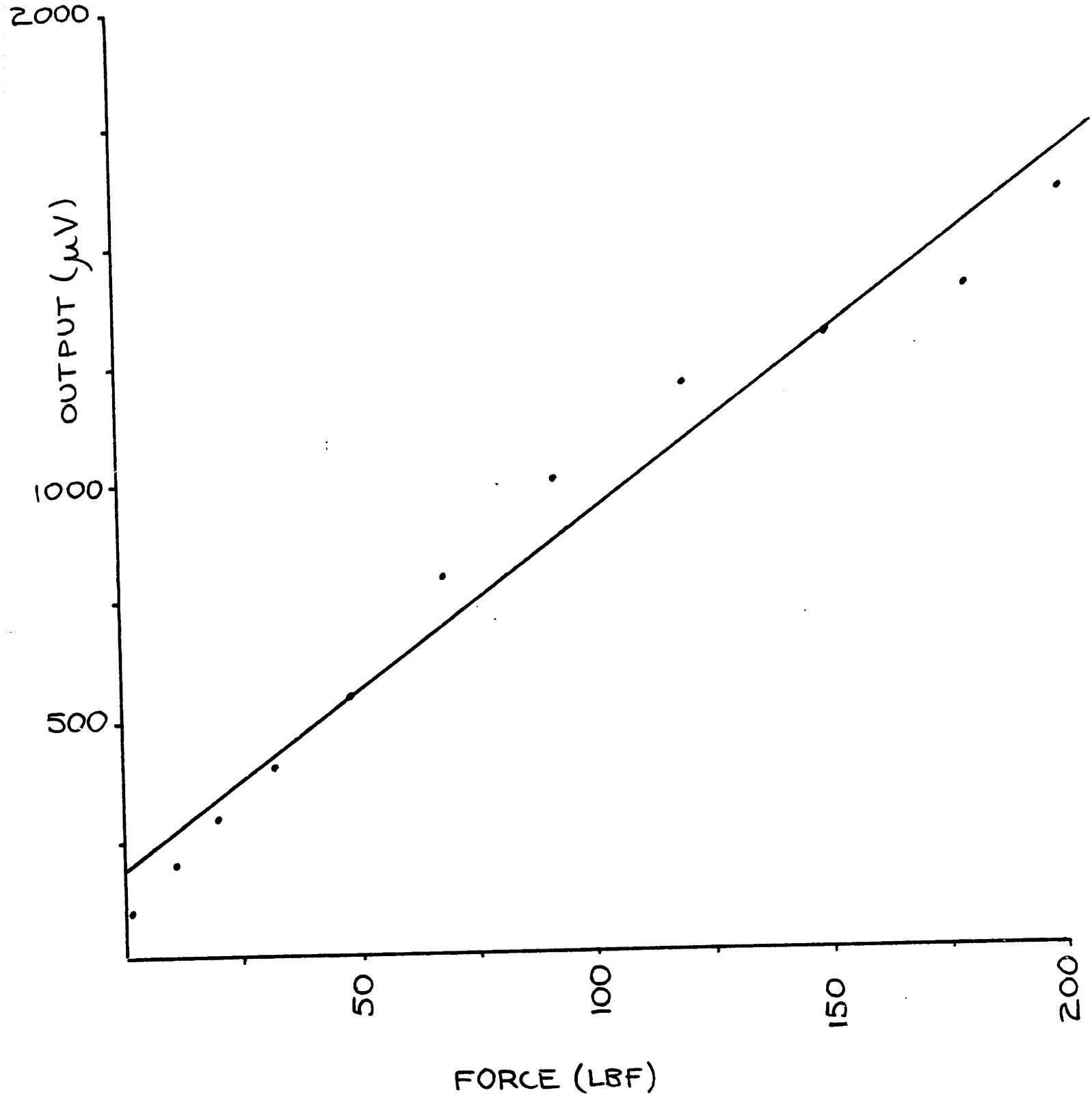

Figure A-10

Calibration Curve for Axial Loading on Half of Load Cell Run 1

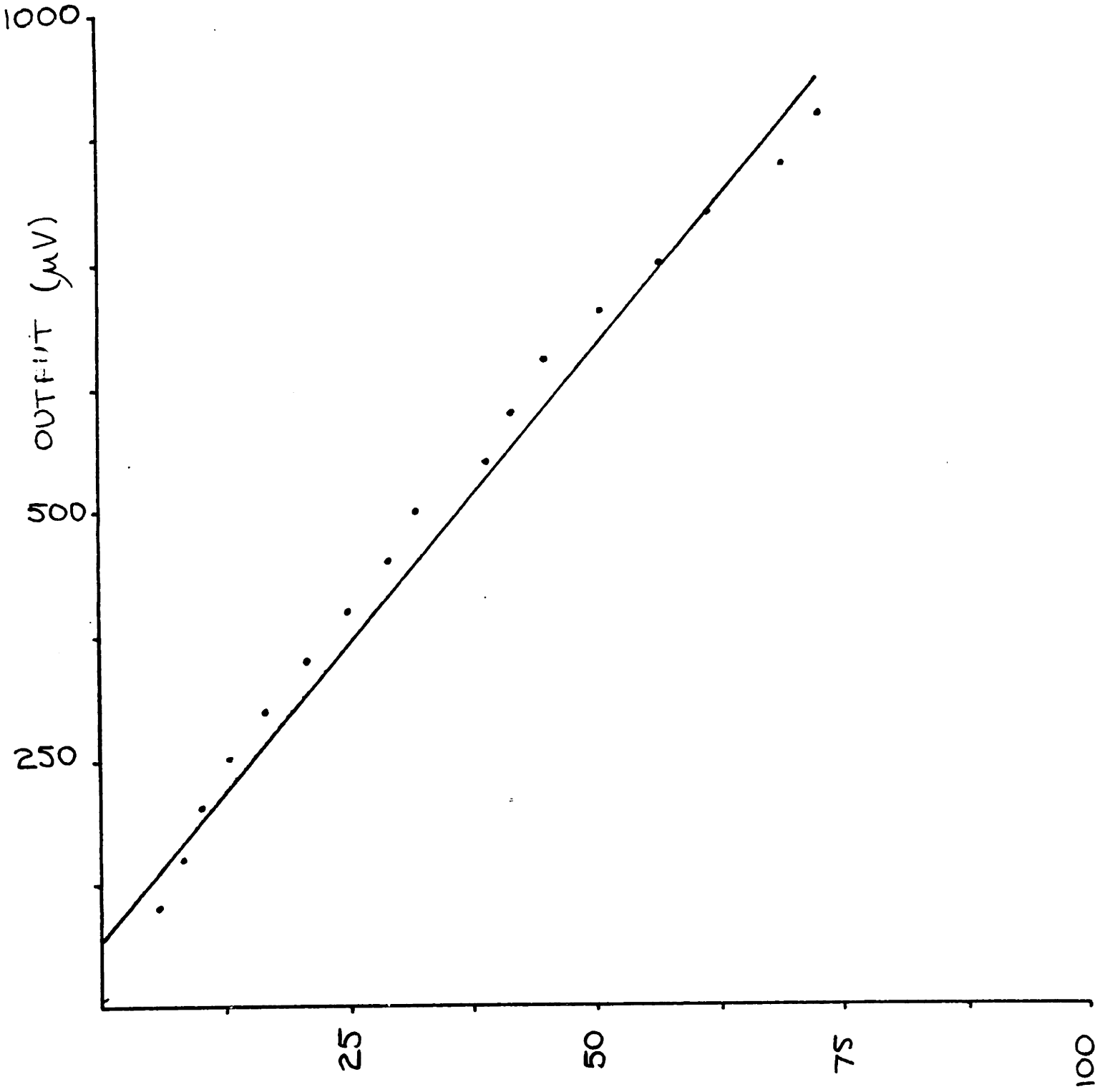

Figure A-11

Calibration Curve for Shear Loading - Run 11

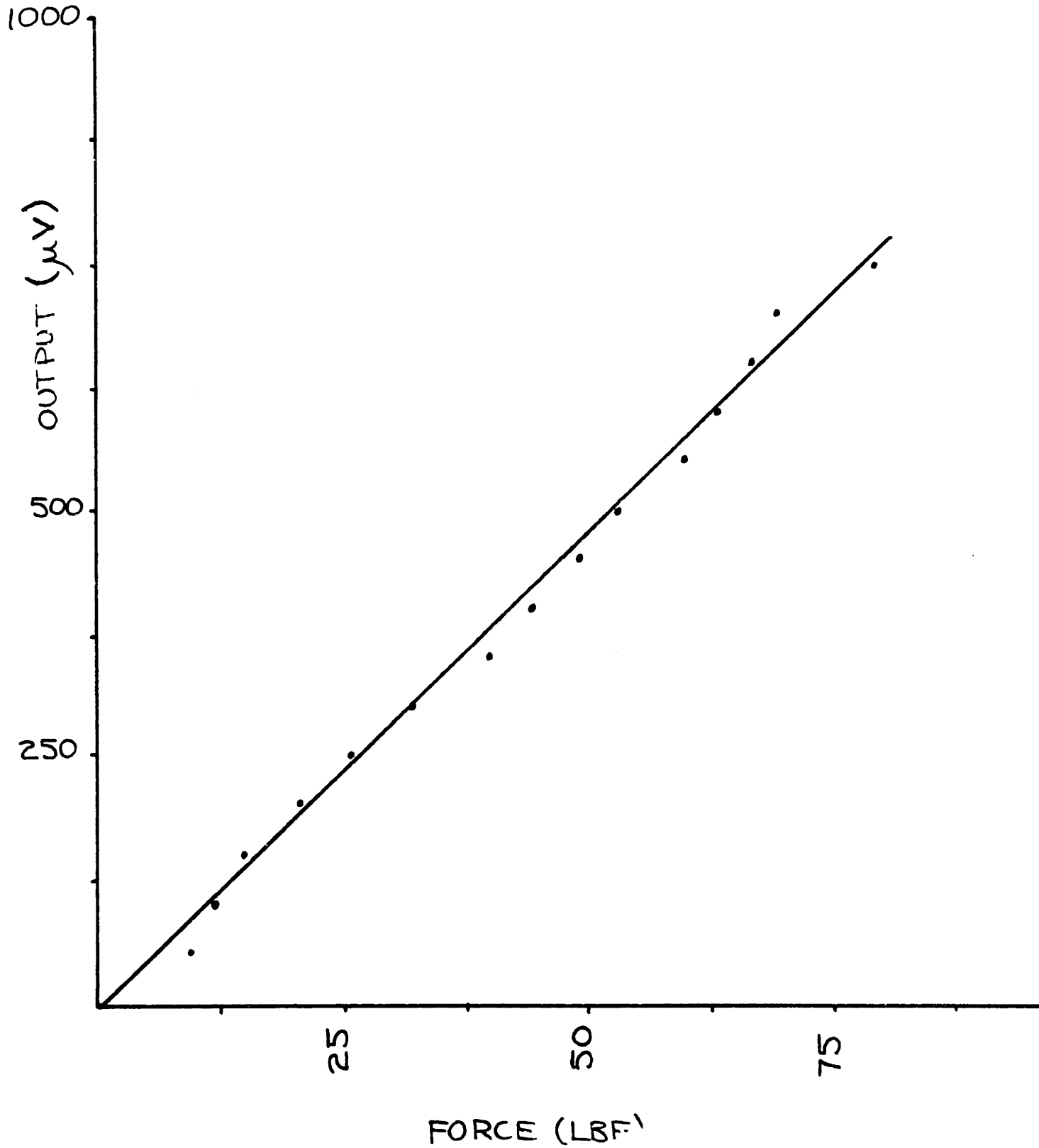

Figure A-12

Calibration Curve for Shear Loading - Run 12

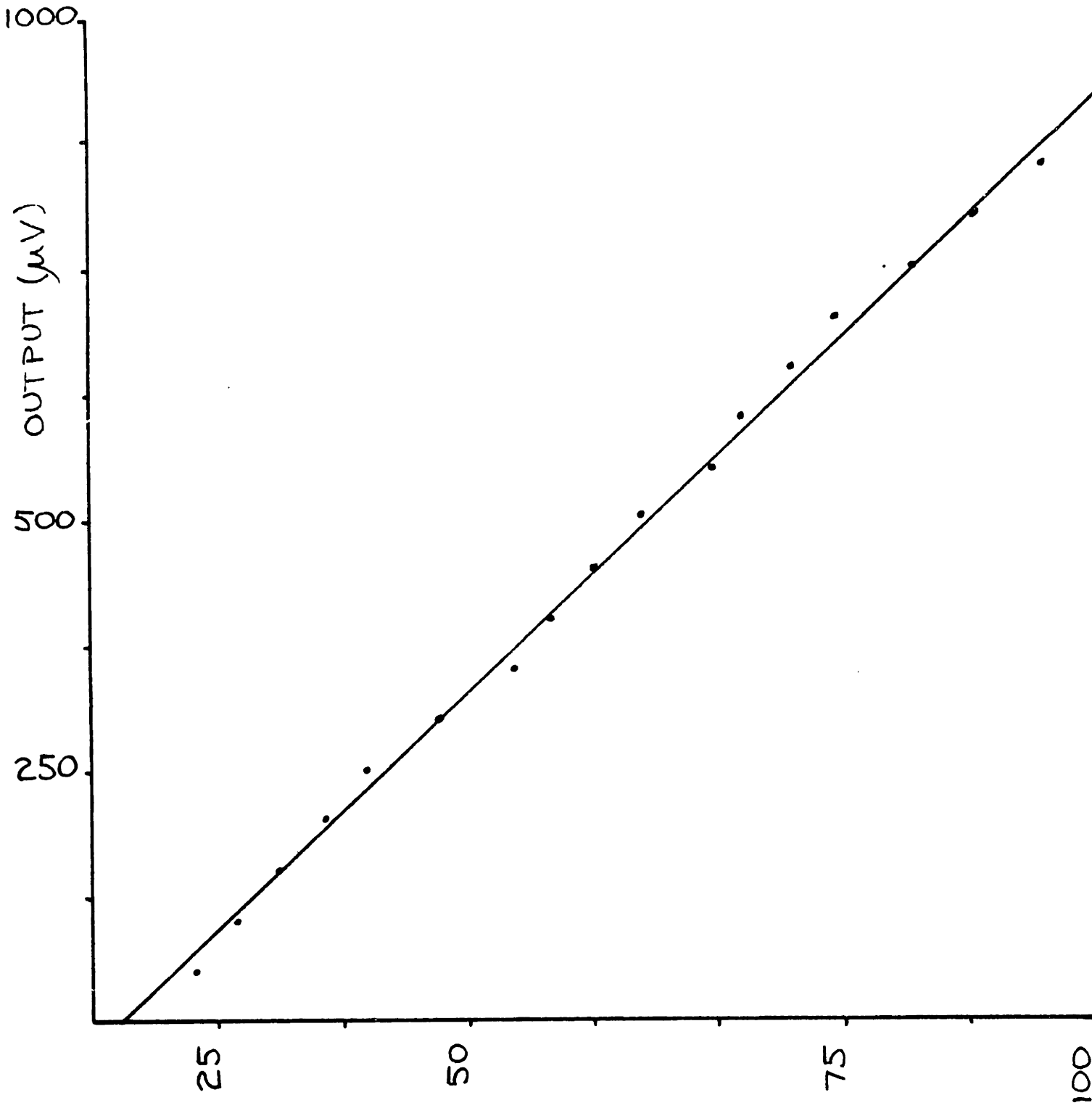

Figure A-13

Calibration Curve for Shear Loading - Run 13

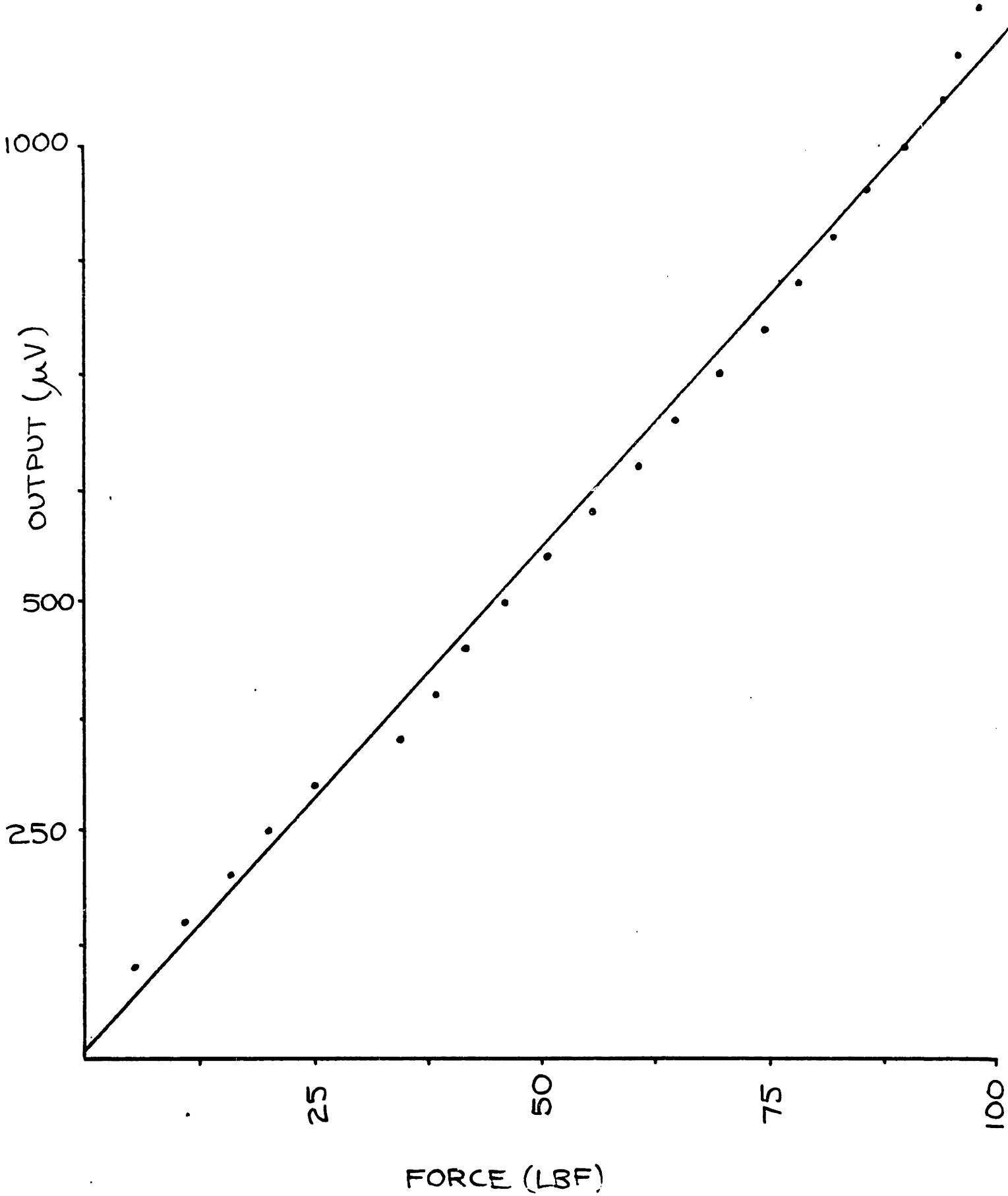

Figure A-14

Calibration Curve for Combined Loading - Run 14

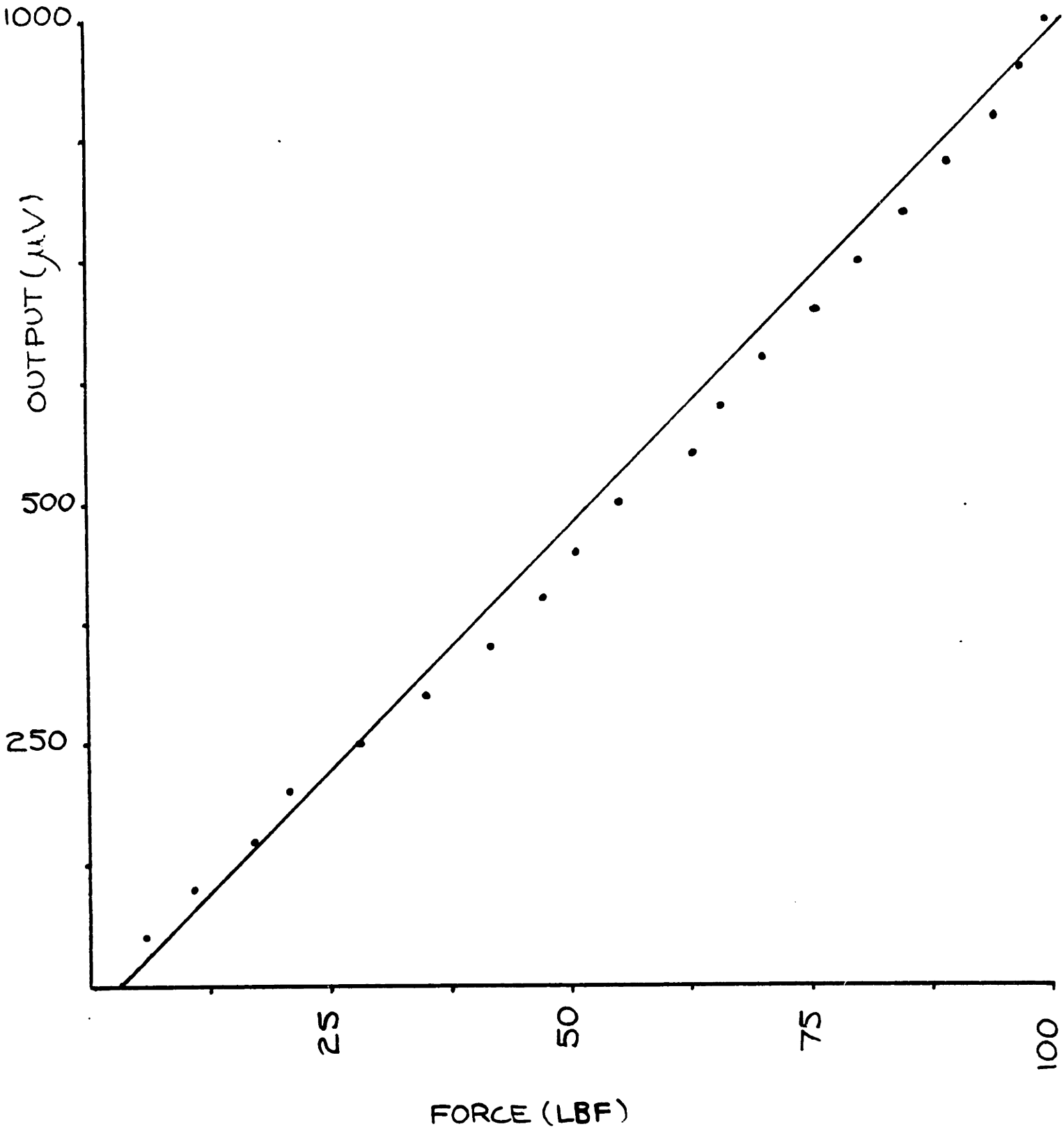

Figure A-15

Calibration Curve for Combined Loading - Run 15

APPENDIX B: LINEARITY ANALYSIS

Scatter diagrams for each run can be constructed as in Figure B-1. The best straight line is drawn to uniformly divide the data points. A least squares linear regression is used to minimize the sums of the squares of the data point deviations from the line of best fit. A linear equation of the form:

$$y = mx + b$$

where: m = slope of line
b = y-intercept of line

is constructed where m and b are determined as follows:

$$m = \frac{\frac{\Sigma x_i y_i}{N} - \Sigma x_i y_i}{\frac{(\Sigma x_i)^2}{N} - \Sigma x_i^2}$$

$$b = \bar{y} - m\bar{x}$$

where: $\bar{x}$ = average x value
$\bar{y}$ = average y value

After the linear regression curve is determined, the degree of association between the random variables can be measured to see how well the linear curve actually fits the data. The linear correlation coefficient r gives this measure:

$$r = \frac{m\sigma_x}{\sigma_y}$$

where: σ_x^2 = variance of the x values = $\frac{\sum x_i^2}{N} - \bar{x}^2$

σ_y^2 = variance of the y values = $\frac{\sum y_i^2}{N} - \bar{y}^2$

There are three other definitions of use in this linear regression analysis. The sensitivity of the function is the response of the output to a change in the input and i simply defined by the slope. Resolution is the input (x) increment that gives some small but definite numerical change in the output (y). The threshold is a minimum value below which no output change can be detected.

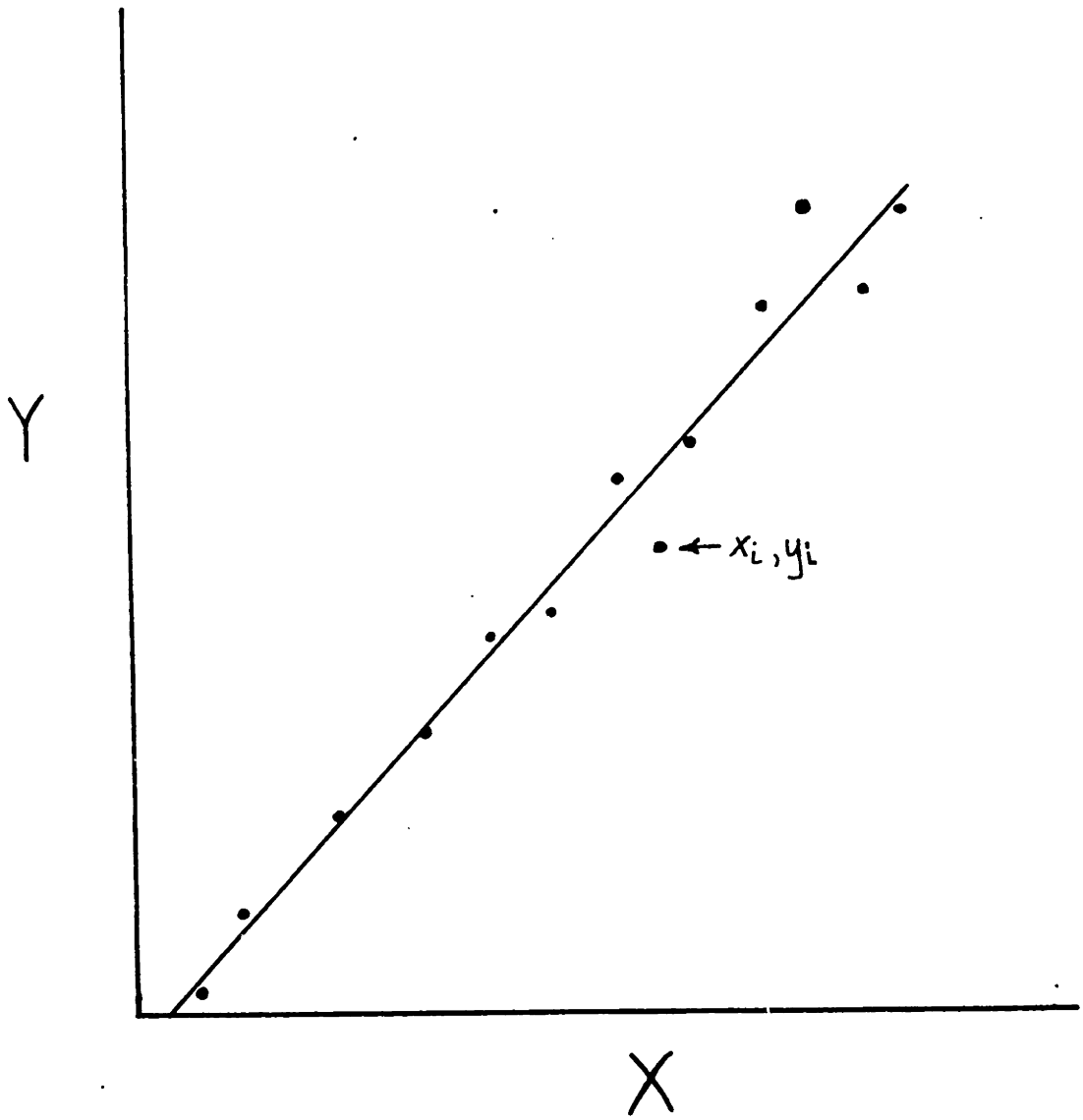

Figure B-1

Scatter Diagram for Best Line Fit

REFERENCES

1. Baumeister, T., Ed; Marks' Standard Handbook for Mechanical Engineers: McGraw-Hill, New York, 1978

2. Ferris, C.; Introduction to Bioinstrumentation: Humana Press, Clifton, New Jersey, 1978

3. Contini, R.; "Body Segment Parameters, Part III", Artificial Limbs, Vol. 16, No 1, 1972, pp 1-19

4. Cook, N.H., Rabinowicz, E.; Physical Measurement and Analysis: Addison-Wesley Publishing Co. Inc., Reading, Massachusetts, 1963

5. Costerus, B.; Transducer Engineer, BLH Electronics, Waltham, Massachusetts

6. Dhanendran, M., Hutton, W.C., Paker, Y.; "The Distribution of Force Under the Human Foot - an on-line Measuring System", Measurement and Control, Vol 11, July, 1978, pp 261-264

7. Doeblin, E.O.; Measurement Systems: Application and Design: McGraw-Hill Book Company, New York, 1975

8. Estey, P.N.; "A Piezoelectric Force Measuring System for Human Moblity Analysis", M.S. Thesis, M.I.T., 1978

9. Frost, R.B., Cass C.A.; "A Load Cell and Sole Assembly for Dynamic Pointwise Vertical Force Measurement in Walking", Engineering in Medicine, Vol 10, No 1, 1981, pp 45-50

10. Hendry, A.W.; Elements of Experimental Stress Analysis: Pergamon Press, Oxford, 1977

11. Holden, T.S., Muncey, R.W.; "Pressures on the Human Foot during Walking", Australian Journal of Applied Science, Vol. 4, 1953, pp. 405-417

12. Lange, C.; "A Preliminary Look at Electrically Conductive Rubber Modules for use in Load Cells", B.S. Thesis, M.I.T., 1976

13. Murray, W., Stein, P.; "Strain Gage Techniques", Lectures at M.I.T., July, 1958

14. Ogata,K.; Modern Control Engineering: Prentice-Hall, Englewood Cliffs, New Jersey, 1970

15. Schaevitz Engineering, Camden, New Jersey

16. Senturia, S., Wedlock, B.; Electronic Circuits and Applications: Wiley and Sons, Toronto, 1975

17. Spolek, G.A., Lippert, F.G.; "An Instrumented Shoe - a Portable Force Measuring Device", Journal of Biomechanics, Vol 9, 1976, pp 779-783

18. Technical Wire Products, Cranford, New Jersey

19. Timoshenko, S.; Strength of Materials: Krieger Publishing Company, Huntington, New York, 1955